Measurement and Fractionation of Diesel Exhaust Hydrocarbons through Variable Temperature Controlled-Condensation and Flame Ionization Detection

A THESIS
SUBMITTED TO THE FACULTY OF
UNIVERSITY OF MINNESOTA
BY

Aaron Serafin Avenido

IN PARTIAL FULFILLMENT OF THE REQUIREMENTS
FOR THE DEGREE OF
MASTER OF SCIENCE

William F. Northrop, Adviser & David B. Kittelson, Co-adviser

May 2014

Acknowledgements

I would like to thank my advisor Dr. William Northrop for his endless support throughout the course of my studies. I learned an incredible amount from him and was continuously inspired by his energy, patience, curiosity and wealth of knowledge. I would also like to thank Dr. David Kittelson for his wisdom and guidance during my time with the Center for Diesel Research; rarely did I leave his office without an answer or a plan to solve the problem at hand. I would also like to thank Dr. Jonathan Chaplin for his support on my thesis committee.

I owe enormous thanks to Glenn Lucachick for his hard work in setting up the GM test cell, his advice throughout the course of the project, and his friendship during long hours in the lab. I would also like to thank the rest of the CDR students and staff for all of their help along the way; especially Dr. Winthrop Watts for his assistance in preparing this thesis. I would like to acknowledge General Motors for their generous gift to the CDR which allowed me to complete my research.

Finally, I would like to thank my family and friends for their unending patience and support; I would not have been able to succeed without them.

Dedication

This thesis is dedicated to the memory of my grandfather, Ronald Herman Dietsche.

Abstract

The industry standard for measuring hydrocarbons in engine exhaust is the flame ionization detector (FID). FID can measure total hydrocarbon concentrations but is limited in that it is not equally sensitive to all hydrocarbons present in exhaust. Instruments capable of measuring individual gas species such as gas chromatography with mass spectrometry (GC/MS) are expensive and sensitive to sample conditioning. A need exists for a simple and relatively inexpensive method to estimate the distribution of lube oil, partially burned, and unburned hydrocarbons present in the exhaust of internal combustion engines.

In this work, a custom-designed variable temperature sample conditioner was developed for use with two fast-response FIDs to determine the condensable fraction of hydrocarbons present in engine exhaust over a range of temperatures. A correction model was developed to compensate for water condensing from the exhaust, nitrogen and carbon dioxide dissolving in the condensing water, and the reduced response factor of a FID in the presence of water. Sample conditioner data processed with the correction model were used to analyze low temperature combustion (LTC) and conventional engine operating modes for diesel fuel and various biodiesel blends.

A theoretical model predicting the condensation of unburned biodiesel as a function of temperature was created using Antoine's equation and was used to validate the hypothesis that the middle weight condensing hydrocarbons were largely unburned fuel. The model was also used to estimate a relative response factor of 0.65 for the unburned

biodiesel, resulting in a response factor of 0.77 for the total HC in the exhaust using the FID tested.

Table of Contents

List of Tables

List of Figures

List of Acronyms

AFR: Air Fuel Ratio

BSFC: Brake Specific Fuel Consumption

CC: Conventional Combustion

CI: Compression Ignited

CO: Carbon Monoxide

CO_2: Carbon Dioxide

DBTDC: Degrees Before Top Dead Center

DOC: Diesel Oxidation Catalyst

DPF: Diesel Particulate Filter

EGR: Exhaust Gas Recirculation

EI: Emissions Index

ELTC: Early Low Temperature Combustion

EPA: United States Environmental Protection Agency

FID: Flame Ionization Detector

FAME: Fatty Acid Methyl Ester

FTIR: Fourier Transform Infrared Spectroscopy

GC: Gas Chromatography

GM: General Motors

HC: Hydrocarbon

HCCI: Homogenous Charge Compression Ignition

HCHO: Formaldehyde

HFID: Hot Flame Ionization Detector

HPLC: High Performance Liquid Chromatography

IC: Internal Combustion

LLTC: Late Low Temperature Combustion

LNT: Lean NO_x Trap

LTC: Low Temperature Combustion

LFE: Laminar Flow Element

NC8: Octane

NMOG: Non-Methane Organic Gases

NO_x: Oxides of Nitrogen

PM: Particulate Matter Mass

RCCI: Reactivity Controlled Compression Ignition

SCR: Selective Catalytic Reduction

SI: Spark Ignited

TCD: Thermal Conductivity Detector

TDC: Top Dead Center

ULSD: Ultra-low Sulfur Diesel

VGT: Variable Geometry Turbocharger

VT: Variable Temperature

1 Introduction

Engine manufacturers focus on reducing engine exhaust emissions to meet United States Environmental Protection Agency (EPA) emissions regulations. US EPA Tier 2 emissions standards for light-duty vehicles are shown in Table 1.1.

Table 1.1: US EPA Tier 2 bin 5 emissions standards given in units of g/mi

	Emission Limits at 50k miles	**Emission Limits at 120k miles**
NO_x (g/mi)	0.05	0.07
NMOG (g/mi)	0.075	0.09
CO (g/mi)	3.4	4.2
PM (g/mi)	-	0.01
HCHO (g/mi)	0.015	0.018

(US EPA 2012)

As of May 2013, the EPA has proposed emissions regulations starting in 2017 to reduce permissible emissions to 20-30% of Tier 2 levels for all emissions demonstrating the continuing trend of ever stricter emissions requirements (US EPA 2013).

Engine manufacturers approach emissions control with three basic strategies: aftertreatment devices, alternative fuels, and in-cylinder modification of combustion. An exhaust aftertreatment system usually contains three devices; a diesel particulate filter (DPF) to control particulate emissions, selective catalytic reduction (SCR) or a lean NO_x trap (LNT) to control oxides of nitrogen (NO_x), and a diesel oxidation catalyst (DOC) to control non-methane organic gases (NMOG) and carbon monoxide (CO) (Johnson 2013).

While these aftertreatment devices are effective in reducing emissions, they are expensive and typically cost around $2000 for light duty vehicles, driving up the price of diesel powered vehicles (Sanchez, Bandivadekar and German 2012).

Alternative fuels such as biodiesel reduce the effective CO_2 emissions due to the CO_2 consumed during growth of the soybean, corn, or other plants or animals used to create the fuel. In addition, biodiesel has been shown to directly lower both soot and gaseous emissions with the exception of NO_x on which it has been shown to have little impact (McCormick, et al. 2006).

Another approach to reduce pollutant emissions is to modify the combustion strategy to prevent pollutant formation. One such approach is premixed low temperature combustion (LTC). Several LTC strategies exist but the overarching principle is to burn a premixed or partially premixed charge at lower local temperatures compared to conventional diesel operation to virtually eliminate the formation of soot and NO_x (Dec 2009). LTC is limited to low to moderate engine loads due to the increased pressure rise rate inherent with compression ignition of a premixed charge (Knafl, et al. 2006). LTC is also characterized by greater incomplete combustion resulting in lower thermal efficiencies and higher CO and hydrocarbon (HC) emissions than conventional combustion (CC).

LTC performance and emissions has been investigated by the University of Minnesota General Motors (GM) project, made possible by the donation of four GM light duty diesel engines and $150,000. Four engine conditions were developed and

characterized, two CC conditions and two LTC conditions. In addition to the characterization of the four engine modes, two projects were generated. The first examines the formation and chemical makeup, specifically the volatile portion, of the particulate matter formed LTC exhaust (Lucachick, et al. 2014).

The second, the focus of this work, examines the composition of the gaseous HCs present in CC and LTC exhaust. The industry standard for HC measurement is the flame ionization detector (FID). FIDs give a measurement of total hydrocarbon concentration and are limited by the types of HCs that can be measured (Martyr and Plint 2012). Different components, especially oxygenated compounds found in biofuels have different FID response factors, complicating their measurement. Other available methods of measuring individual HC components such as Fourier transform infrared spectroscopy (FTIR) or gas chromatography (GC) are expensive and or limited in the quantity of species they can measure.

This work addresses four objectives: 1) Demonstrate a low-cost online method to determine the relative volatility of HC emissions; 2) Use this technique to compare the volatility of HCs in the exhaust from conventional diesel combustion to low temperature combustion modes and conventional diesel fuel to various biodiesel blends; 3) Use the generated volatility profile to identify three distinct groups of HC components in the exhaust; and 4) Create and use a condensation model of biodiesel to determine a relative response factor for the biodiesel contribution to HC emissions in exhaust.

2 Background

2.1 Emissions Standards

Emissions standards for heavy duty and light duty engines are established by the EPA. Table 1.1 shows Tier 2 emissions standards. These standards apply to light duty vehicles and are given in g/mi. For this research it is more convenient to refer to the emissions standards by an emissions index (EI) or g/kg of fuel as the engine tested is stationary and not installed in a vehicle. Table 2.1 gives the Tier 2 emissions limits in g/kg of fuel for various fuel economies using Equation 2.1 and where S_i is the emissions standard, FE is the fuel economy, and ρ_{fuel} is the density of diesel, 0.85 kg/L (Northrop 2010).

$$EI_i\left(\frac{g}{kg_{fuel}}\right) = S_i\left(\frac{g}{mi}\right) FE\left(\frac{mi}{gal}\right)\frac{1}{3.785}\left(\frac{gal}{liter}\right)\frac{1}{\rho_{fuel}}\left(\frac{L}{kg}\right)$$

Equation 2.1

The conversion from the EPA standard in g/mi to g/kg-fuel assumes a constant fuel economy and does not take into account the drive cycle on which the EPA standard is based.

Table 2.1: US-EPA Tier 2 emissions standards in g/kg-fuel

Fuel Economy (mi/gal)	**25**	**30**	**35**	**40**	**45**	**50**
NO_X	0.54	0.65	0.76	0.87	0.98	1.09
NMOG	0.70	0.84	0.98	1.12	1.26	1.40
CO	32.64	39.16	45.69	52.22	58.75	65.27
PM	0.08	0.09	0.11	0.12	0.14	0.16
HCHO	0.14	0.17	0.20	0.22	0.25	0.28

EPA Tier 3 emissions standards which will be phased in from 2017 to 2025 (US EPA 2013) can be found in Table 2.2. Tier 3 standards have reduced the permissible levels of all emissions to roughly 25% of their Tier 2 values and 2-3% of their Tier 1 values, demonstrating the continuing trend of stringent emissions standards that will continue to push engine manufacturers to develop more effective engine emissions control strategies.

Table 2.2: US EPA Tier 3 emissions standards in g/kg-fuel

Fuel Economy (mi/gal)	**25**	**30**	**35**	**40**	**45**	**50**
NO_X+NMOG	0.23	0.28	0.33	0.37	0.42	0.47
CO	7.77	9.32	10.88	12.43	13.99	15.54
PM	0.02	0.03	0.03	0.04	0.04	0.05
HCHO	0.03	0.04	0.04	0.05	0.06	0.06

Tier 3 standards also combine NO_X and NMOG into a single quantity. EPA defines NMOG as “the sum of oxygenated and non-oxygenated hydrocarbons contained in a gas sample” (US EPA 2014). For EPA testing for diesel vehicles NMOG is calculated by

summing the mass of non-methane hydrocarbons (NMHC) measured using FID with a methane cutter and the mass of carbonyls measured using impinger samples and high performance liquid chromatography (HPLC). NMHC is determined by measuring total HC using FID and subtracting methane, measured using GC-FID (Air Resources Board 2012).

2.2 Introduction to Internal Combustion Engines

Internal combustion (IC) engines have played a crucial role in the development of modern society. Since their development in the 19th century, the IC engine has remained the staple for mobile power generation. Even with technological advancements in electrics and hydraulics made in recent years, the ability of IC engines to convert high energy density combustible fuels into useful work remains irreplaceable in a wide variety of applications.

The two most common types of internal combustion engines are spark ignited (SI) engines and compression ignited (CI) engines. Both function under similar principles; a combination of fuel and air is combined in a cylinder, compressed, and burned. The burning of the fuel air mixture increases the pressure in the cylinder, moving a piston connected to a crank shaft, outputting useable work. The difference between the two forms is the source of ignition, which dictates the type of fuel used.

In an SI engine, traditionally a stoichiometric mix of fuel and air are combined prior to being drawn into the cylinder. The engine load is controlled by throttling the quantity of the mixture drawn into the cylinder. The mixture is then compressed and

combustion is initiated near top dead center using a spark. Since the premixed charge of fuel and air is mixed prior to being compressed, the temperature and pressure in the cylinder increase. If the temperature and pressure get too high, the fuel and air charge can auto-ignite, in a damaging event called knock. To avoid knock, the compression ratio of SI engines is limited and a low reactivity fuel such as gasoline is used. SI engines generally run on a stoichiometric mixture of fuel and air. The engine load is controlled by throttling the intake of this fuel air mixture into the engine.

While auto-ignition is avoided in SI engines, it is the principle initiating combustion in CI engines. In a CI engine, un-throttled air is drawn into the cylinder and compressed. A high reactivity fuel such as diesel is then injected into the hot, compressed air shortly before top dead center (TDC). The mixture auto-ignites due to the high temperatures and continues to burn as it is injected. The use of CI allows for higher compression ratios. The higher compression ratios and lower pumping losses due to a lack of throttling resulting in overall higher efficiencies for CI engines over SI engines. Whereas SI engines burn a stoichiometric mixture of fuel and air, a CI engine draws in unthrottled air and load is controlled by the quantity of fuel injected. This results in a globally lean charge that is not premixed, resulting in heterogeneous combustion and different zones of burning as seen in Figure 2.1.

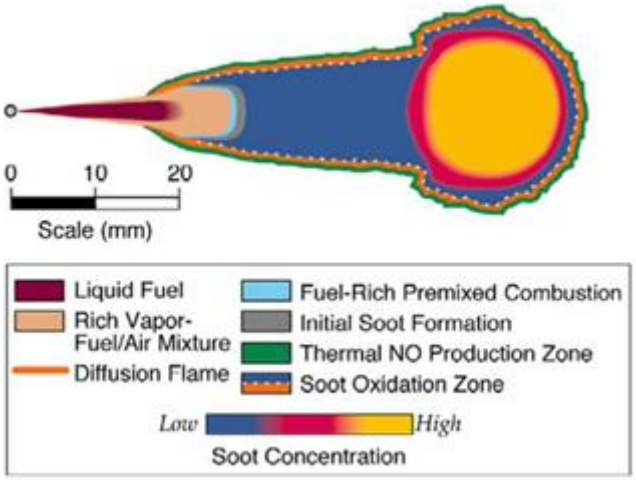

Figure 2.1: Compression ignition burning profile (Dec 2009)

The resulting diffusion flame is responsible for the formation of soot, NO_X, CO, and unburned and partially burned HC. Soot is formed when fuel is not completely oxidized such as in fuel-rich zones. NO_X is formed from nitrogen and oxygen reacting in high temperature environments. Lean zones in CI engines are suitable for NO_X formation due to the high temperatures of combustion and the presence of excess oxygen. While typically very low in CC, both rich and lean zones are responsible for the formation of unburned and partially burned HCs. Heywood (1988) and others have shown that CO and HC are formed due incomplete burning of over-mixed lean regions, under-mixed rich regions and formed from flame quenching on the piston and cylinder walls.

Avoiding the formation of these different emissions is a delicate task. Kamimoto and Bae (1988) investigated the engine conditions in which soot and NO_x were formed and generated a map shown in Figure 2.2 defining two distinct regions.

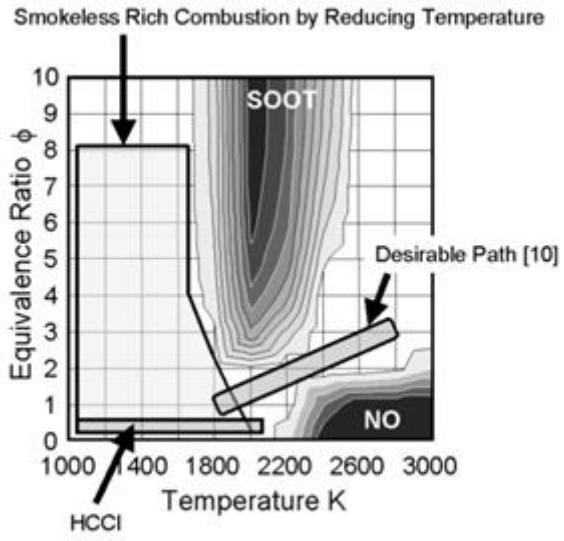

Figure 2.2: Emissions formation as a function of local temperature and equivalence ratio (Akihama, Takatori and Inagaki 2001)

As shown in Figure 2.2, NO_X is formed at moderate equivalence ratios and local temperatures above 2100 K and soot is formed above local equivalence ratios of 2. CC takes place in a region encompassing both the soot zone and the NO_X zone. In CC, attempting to mitigate soot formation by decreasing the equivalence ratio generally increases the local temperatures, increasing NO_X formation. The opposite is also true; increasing equivalence ratio to reduce combustion temperatures leads to an increase in soot formation. This is traditionally known as the soot-NO_X tradeoff (Stone 1999). LTC attempts to defeat the soot-NO_X tradeoff by operating in the zones defined in Figure 2.2.

2.3 Low Temperature Combustion

One method widely used in production diesel engines to reduce NO_X formation is exhaust gas recirculation (EGR) (Stone 1999). Engines using EGR have a circuit that

takes a fraction of the engine exhaust and reroutes it into the intake manifold. This introduction of combustion byproducts dilutes the fresh air charge, and increases the heat capacity of the mixture, reducing the overall combustion temperature. While EGR has been shown to be effective in reducing NO_X, engine manufacturers have not been able to use EGR alone to meet EPA emissions regulations without the addition of exhaust aftertreatment devices.

There are several alternative combustion modes focused on preventing emission formation in situ. As seen in Figure 2.2, Kamimoto and Bae (1988) identified a "desirable path" corresponding to high temperature combustion in which temperatures are high enough to oxidize any soot formed and the equivalence ratio rich enough where the lack of oxygen inhibits NO_X formation. Also identified in Figure 2.2 is a "smokeless rich combustion by reducing temperature" zone in which temperatures are low enough to prevent the formation of soot and NO_X. This LTC regime is the region in which the experiments of this work were performed.

The underlying principle of LTC is to use injection timing and duration to control ignition delay. By increasing ignition delay the fuel and air have more time to mix, resulting in reduced local equivalence ratios and combustion temperatures, therefore inhibiting soot and NO_X formation. Several strategies exist to achieve LTC conditions.

Homogeneous charge compression ignition (HCCI) is the most ideal form of LTC but poses several challenges. In HCCI operation, a high reactivity fuel such as diesel fuel is injected early to allow for the charge to sufficiently mix. The globally lean

homogeneous charge is then compressed and small kernels of near-stoichiometric conditions spontaneously auto-ignite across the entire cylinder. While this operation reduces NO_X due to the low temperature associated with the globally lean conditions and reduces soot due to the premixed charge, HCCI is difficult to control as it lacks an event to control ignition, such as a spark in SI or the fuel injection in CI (Franklin 2010).

The LTC performed here can be referred to as early LTC (ELTC) and late LTC (LLTC). These two strategies fall into the "smokeless rich combustion by reducing temperature" zone of Figure 2.2. In both conditions extremely high levels of EGR (up to 60%) are used to significantly dilute the fuel air mixture and further increase ignition delay. High injection pressures are also used to enhance fuel and air premixing. In ELTC fuel is injected 10-15° earlier in the compression stroke than in CC. In the work performed here, fuel was injected around 20 ° before TDC (DBTDC). This early injection allows the fuel to partially premix before ignition occurs. Partial premixing reduces rich zones, significantly limiting soot formation. The heavily diluted charge also keeps combustion temperatures sufficiently low to inhibit NO_X formation. As the level of mixing increases, the rate of burning and therefore the pressure rise rate and combustion noise increases. To avoid knock resulting from rapid pressure rise rates, ELTC is limited to low load conditions (Knafl, et al. 2006).

During LLTC, fuel is injected just before TDC (around 3 DBTDC) but due to the highly dilute mixture of air and exhaust gases ignition delay is extended and combustion continues into the expansion stroke. This allows for partial premixing of the charge and

lower combustion temperatures. Having the bulk of the combustion occurring during the expansion stroke, the pressure rise rate issue associated with ELTC is avoided allowing LLTC to be used up to 7 bar BMEP. Above 7 bar BMEP, the longer injection duration required for increased load does not allow time for premixing resulting in more diffusion burning and unacceptable levels of soot production (Knafl, et al. 2006).

LTC modes are not without complications. In addition to the limited loads, the highly dilute low temperature conditions lead to incomplete combustion resulting in decreased combustion efficiency. And while soot and NO_X are practically eliminated, CO and HC emissions increase dramatically. In CC, exhaust HCs are treated by oxidizing them using a DOC which is most active with catalyst inlet temperatures greater than 250 °C. The exhaust temperatures resulting from LTC are much lower than those from CC resulting in greater difficulty using a DOC to treat HC and CO emissions. To overcome these challenges, the sources of HC in LTC must be identified.

HCs in engine exhaust result from three sources: unburned fuel, partially burned fuel, and lubricating oil. Greeves et al. (1977) and Koci et al. (2006) have shown that the fuel remaining in the injector sac is responsible for much of the unburned HC in both CC and LTC exhaust. In addition, the advanced timing and high pressure of the fuel injection associated with LTC result in high pressure unburned fuel being sprayed into a lower pressure environment than in CC resulting in unburned fuel being deposited in the piston top-land crevice as well as on the piston-top and cylinder walls that later vaporize in the expansion stroke (Kashdan, Mendez and Gilles 2007) (Dec 2009).

The levels of partially burned HC are also higher for LTC than CC. In CC and LTC alike, flame quenching at the cool cylinder walls results in unburned HC (Heywood 1988); however, in LTC, bulk gas quenching occurs due to zones where the temperature is too low, or the equivalence ratio is too rich, or too lean for complete combustion to occur (Lewis, Storey and Bunting 2005) (Kashdan, Mendez and Gilles 2007). These fuel-rich and fuel-lean zones have been investigated by Musculus, et al. (2007), who showed since the injection event is completed before ignition, after the injection event is completed, the momentum of the fuel being injected entrains ambient gases resulting in a fuel-lean zone near the injector as seen in Figure 2.3. Figure 2.3 also shows that while the majority of the charge is pre-mixed some soot producing fuel rich zones still remain.

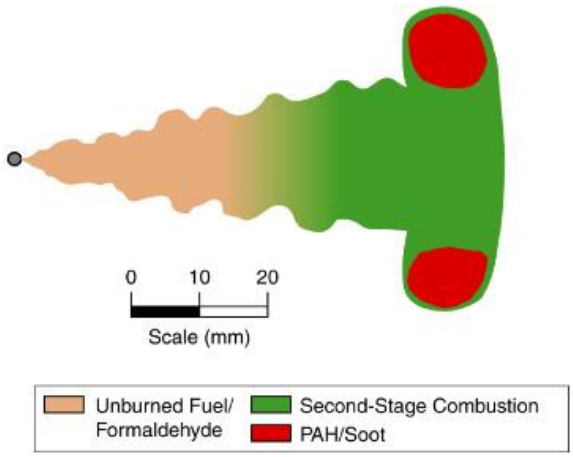

Figure 2.3: Low temperature combustion burning profile (Musculus, et al. 2009)

2.4 Hydrocarbon Measurement Challenges

The variety of approaches that exist for controlling emissions creates a need for methods to compare the effect of each approach. HC concentration in engine exhaust is

typically measured by a FID. Traditional FID and fast response FID instruments both consist of a hydrogen and air flame and a detector electrode (McWilliam and Dewar 1958) (Cheng, Summers and Collings 1998). Exhaust is drawn into the hydrogen-air flame and burned. The burning of exhaust HCs in the hydrogen and air diffusion flame generates ions which are drawn towards the voltage biased detector electrode. As the ions impact the electrode a current is generated that is proportional to the number of ions collected and therefore proportional to the number of ions generated in the flame. It has been shown that the number of ions generated is directly proportional to the HC concentration in the gas being burned (McWilliam and Dewar 1958).

Several FID combustion mechanisms have been suggested since McWilliam and Dewar demonstrated the original FID concept; however, the generally accepted primary method of ion formation is due to the chemi-ionization reaction suggested by Calcote, shown in $CH + O \rightarrow CHO^+ + e^-$ Equation 2.2 (Calcote 1961).

$$CH + O \rightarrow CHO^+ + e^- \qquad \text{Equation 2.2}$$

During the initial stages of combustion in a FID diffusion flame, prior to being oxidized, hydrocarbon chains are broken down into radicals which are quickly created and destroyed. This rapid destruction and creation of radicals removes the identity of the individual hydrocarbon chains, creating an indiscriminate "pool" of radicals (Schofield 2008). Depending on the conditions of the flame, a certain fraction of the decomposed hydrocarbon chains will form CH radicals which react with O in $CH + O \rightarrow CHO^+ + e^-$ Equation 2.2 resulting in the formation of the CHO^+ ion. A certain fraction of these

CHO^+ ions generate a current when captured by the detector electrode. This current is proportional to the total number of carbon atoms present in the hydrocarbon structures contributing to the radical pool (Schofield 2008). As a result, FID is only suitable for measuring the total HC concentration in the exhaust.

While accurate for alkanes, alkenes and other non-oxygenated HCs, difficulties exist for measuring oxygenated compounds such as biodiesel as they have a reduced FID response. Whereas aliphatic HCs are uniformly broken down, generating a concentration of CH proportional to the initial carbon content of the HC, the oxygenated groups present in FAMEs create complications. The carbon-oxygen bonds present in oxygenated hydrocarbons remain intact throughout combustion, creating CO (Schofield 2008). Since CO oxidation does not follow a chemi-ionization kinetic route though CH, the carbon atom bonded to an oxygen atom is thus not detected. As alternative fuels such as biodiesel gain popularity, the complications of measuring the exhaust generated by burning these fuels becomes increasingly important.

Biodiesel is composed of a variety fatty acid methyl esters (FAMEs) produced by transesterification. Fats and oils from plants or animals are combined with alcohols in the presence of a catalyst to break up the triglycerides into FAMEs and glycerin. The glycerin is removed and the resulting FAMEs are oxygenated hydrocarbons that are chemically similar to the HC chains found in conventional diesel fuel allowing biodiesel to be blended with conventional diesel fuel (Bart, Palmeri and Cavallaro 2010). However,

its oxygenated nature results in a reduced response factor for measurement of unburned fuel from incomplete combustion when using FID.

Schreiner and Hulan (2004) and others have proposed theoretical methods calculating the response factor for oxygenated compounds by determining an effective carbon number by subtracting a certain value for each oxygen containing chemical structure within the chain from the total carbon number for the specific HC. However, Badings and De Jong (1983) as well as the US EPA (2014) recommend determining empirical response factors for individual systems using calibration gases of oxygenated compounds as the specific flame for each configuration is unique.

Since FID only gives a measurement of total HC, instruments other than FIDs must be used to determine the concentration of individual HCs. GC analysis can accurately measure a vast variety of individual HCs and other compounds. A sample is evaporated in a carrier gas such as helium, argon, or nitrogen and then sent through a capillary or packed bed column coated with a stationary phase. As the sample is drawn through the column the different species in the sample interact with the stationary phase causing them to be drawn through the column at different speeds. As a result there is a distribution of times required for different components to elute from the column. The different retention times correspond to different species. After passing through the column the components are measured with one of several detectors, usually either a thermal conductivity detector (TCD) or FID, generating a distribution of the concentration of different compounds. GC can also be used with a mass spectrometer (GC-MS) to further differentiate between

groups of species that elute at the same time in the column (Blumberg 2012). While accurate, GC instruments are expensive and special care must be taken to ensure the components entering the GC are sufficiently diluted to ensure they remain in the gas phase and since a known volume must be injected and timed, measurements cannot be taken in real time.

Another method of identifying individual hydrocarbon components is FTIR. FTIR works by measuring the amount of infrared light absorbed at a variety of wavelengths. Different gas species absorb different wavelengths of infrared light. The amount of light absorbed at a specific wavelength is dependent on the concentration of that species in the gas sampled. Therefore by sweeping over a range of infrared wavelengths, the FTIR is able to measure the concentration of a variety of gases. The FTIR is able to sweep through wavelengths extremely quickly, generating a spectrum, allowing for the FTIR to measure different gases including, but not limited to, CO_2, H_2O, NO_X, and a variety of other important exhaust components in real time (AVL 2013). However, FTIR is only able to accurately measure light hydrocarbons and thus is not useful for total hydrocarbon measurement diesel exhaust.

A need exists for a low cost, simple method to further discretize exhaust HCs. Andrews et al. (2000) developed a method to determine different fractions of HC based on temperature using several separate FIDs: one hot Fast FID near the exhaust manifold, a FID operating at 180° C, a FID operating at 50° C, a FID operating at 2° C and a non-methane hydrocarbon analyzer to determine the methane fraction. This setup offers the

ability to measure three component groups of HCs: in an online method; however, it requires the use of at least three FIDs. In addition, Andrews et al. filtered out particulate at each specified temperature allowing for the removal of hydrocarbons that had condensed on particulate before filtration. In this method the soluble organic fraction of PM was estimated.

It is of interest to know the fraction of HCs condensing at a wider range of temperatures without particulate interaction to determine the relative volatility of the gaseous HCs generated. The work presented here extends the research conducted by Andrews et al. by increasing the number of temperatures sampled to determine the condensable fraction of exhaust HC to any temperature in the range of 20° to 191° C.

3 Methods and Materials

3.1 Engine

A 2.0L GM A20DTH Euro V emissions certification turbocharged diesel engine was used to produce the exhaust emissions analyzed in this study. The engine was coupled to an eddy current dynamometer. The A20DTH was equipped with high pressure common rail direct injection, a variable geometry turbocharger (VGT), and EGR. The engine dimensions and specifications are located in Table 3.1.

Table 3.1: GM A20DTH Engine specifications

Number of Cylinders	4
Displacement, cc	1956
Bore, mm	83.0
Stroke, mm	90.4
Compression Ratio	16.5:1
Power output kW/rpm	117.3/4000
Torque Nm/rpm	350/1750
Emissions Rating	Euro V
Fuel System Maximum Pressure	160 MPa

3.2 Engine Modifications

In its factory configuration, the A20DTH meets Euro V and US EPA Tier 2 emissions standards. The stock aftertreatment system was removed and raw exhaust was sampled and analyzed for this work. An aftermarket aftercooler was added with an external coolant loop to provide control over the intake air charge temperature. The stock EGR cooler was also modified to provide a wider range of temperature control. A custom bypass manifold was machined to remove the EGR circuit from the engine coolant loop and add an external water supply to the EGR cooler to control the output temperature of the EGR, and therefore the intake manifold, over a wide range of temperatures. A sample port for measuring gaseous emissions was also installed on the intake manifold.

The engine was equipped with a National Instruments DRIVVEN control system, replacing the manufacturer equipped engine control unit. The use of the DRIVVEN

system in tandem with National Instruments Combustion Analysis System (NI-CAS) allowed for full control over all engine parameters including but not limited to number of fuel injections, fuel injection timing, fuel injection duration, EGR valve position, VGT position, variable swirl actuator (VSA) position, fuel rail pressure, and throttle position.

3.3 Instrumentation

Data Acquisition and Engine Control

A National Instruments system consisting of a NI-PXI 1050/SCXI-1001 combination chassis controlling a TC-2095 thermocouple connector block and a BNC-2095 BNC connector block for 2 Hz low speed data collection. In addition a BNC-2090A BNC connector block was used for high speed data acquisition of factory supplied Borg-Warner glow plug pressure transducers and a BEI H25 encoder.

Fuel and Air Flow

The intake air volumetric flow rate was measured using a 50MC2-4 Meriam laminar flow element (LFE) and the mass flow rate of fuel was measured using a Micro Motion Coriolis flow meter. Figure 3.1 shows a schematic of the fuel delivery and flow measurement system.

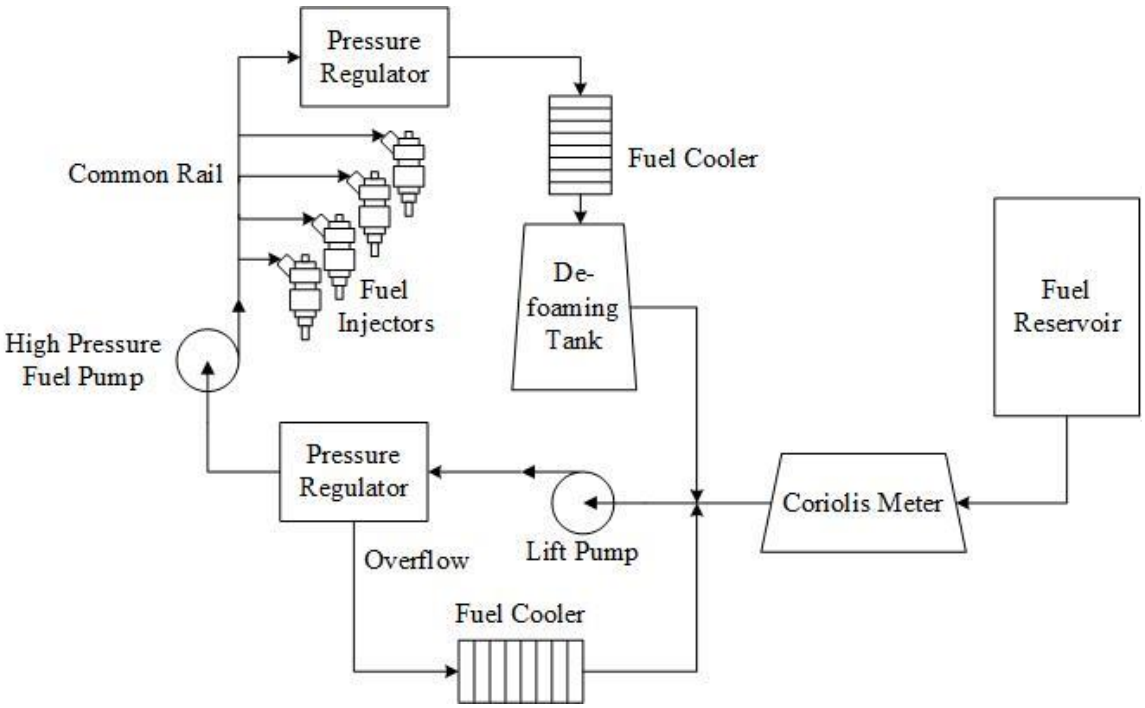

Figure 3.1: Fuel delivery system

The emissions measurement system was arranged as shown in Figure 3.2. For all the exhaust samples taken, stainless steel probes with 45° cut beveled ends open to the centerline of the flow were used. All heated lines and filters were maintained at 191° C as specified by EPA (185°-197° C) (US EPA 2011).

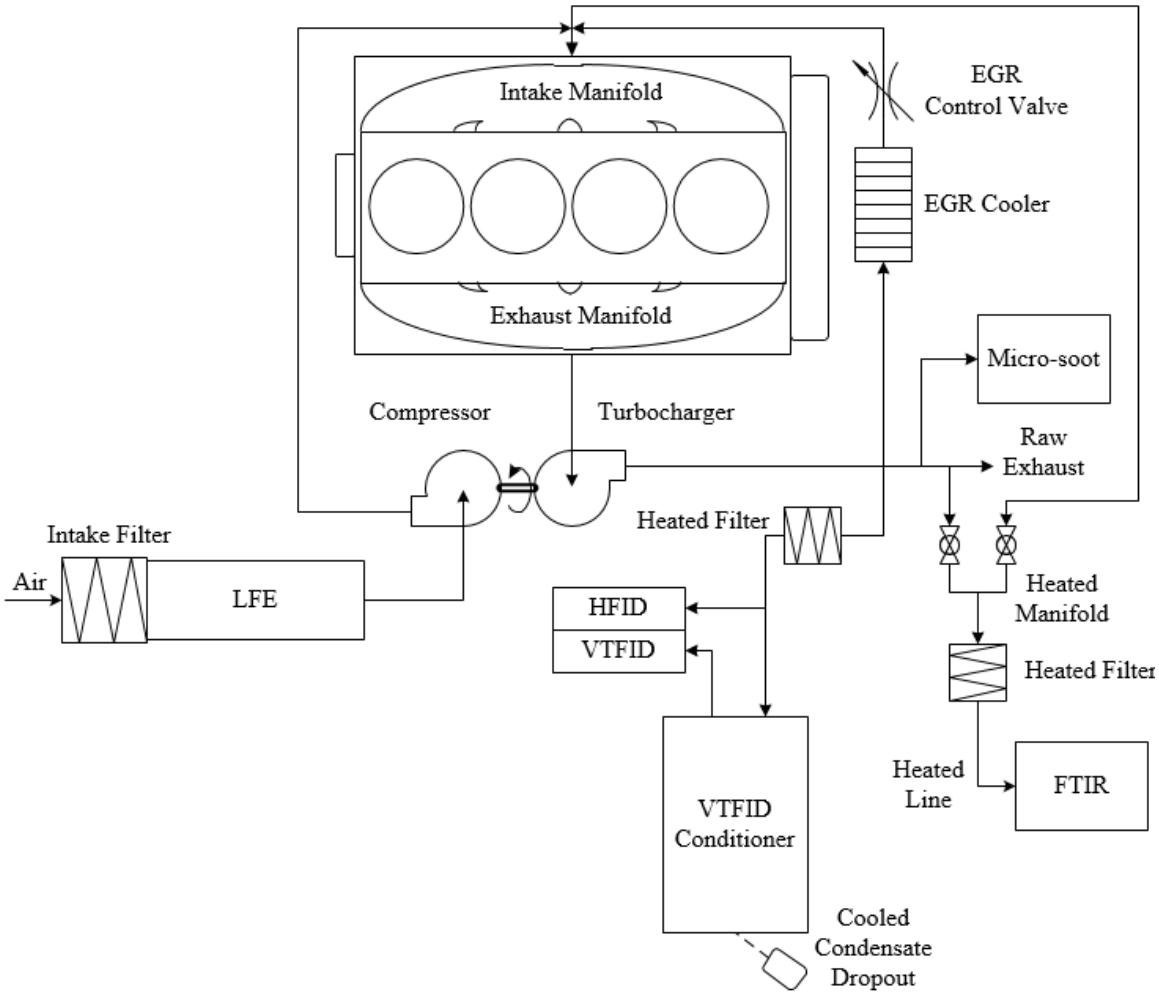

Figure 3.2: Emissions flow diagram

Hydrocarbon Measurement

A Cambustion HFR500 two channel fast FID was used to measure the HC concentration of raw exhaust and the HC concentration of conditioned exhaust. A fast FID operates under the same principle as a conventional FID with modifications. In a conventional FID a sample pump draws a sample through a heated sample line from the

source to the detector located in the instrument. The detector in a fast FID is located on the end of the heated sample probe and is therefore much closer to the sample source. This minimizes sample losses and the time it takes the sample to move from the source to the detector. The sample is also under much higher vacuum allowing the FID to have a response as fast as 0.7 ms (Cambustion 2014).

The first FID channel measured the total HC concentration at 191° C upstream of a custom built variable temperature (VT) sample conditioner. The second FID channel measured downstream of the sample conditioner which was varied from approximately 20° C to 191° C. The difference between the two FID measurements represents the fraction of HCs condensing at the temperature of the sample conditioner.

Variable Temperature Sample Conditioner Principles

The main principle behind the VT sample conditioner is that as the exhaust gas cools, different components (specifically HCs) present in the exhaust stream condense and are stored in the conditioner. Condensation of a component will occur when the temperature of the exhaust gas falls below the component's dew point; the temperature at which the exhaust gas stream is saturated with a component. The concentration of a component in the mixture at its dew point is known as the saturation concentration. The concentration is also the ratio of the absolute partial pressure of the component to the absolute pressure of the mixture. This partial pressure corresponding to the dew point is the vapor pressure.

If the gas is saturated with a component and exposed to a surface at a temperature below its dew point, that component will condense onto the surface. In the case of the VT sample conditioner, as the conditioner cools, the walls of the conditioner fall below the dew points of various components in the exhaust, causing them to condense on the walls of the conditioner and be collected.

Variable Temperature Sample Conditioner Design

The sample conditioner was designed to accurately control sample temperature from room temperature (20°C) to the EPA defined line temperature for measuring HCs (191°C) (US EPA 2011). It was determined that the flow through the sample conditioner was laminar as calculated by the sample flow rate of 3 L/min and the sample passage diameter of ¼" ID. Assuming the inner surface of the sample line was at a constant temperature, $h = \frac{k_f Nu_D}{D}$ Equation 3.1 through $L = \frac{q}{h\pi D T_{lm}}$ Equation 3.4 were used to solve for L the required length of variable temperature sample line necessary to cool the sample at temperature T_{in} to the desired outlet temperature, T_{out}. Where h is the convective heat transfer coefficient of the fluid, k_f is the thermal conductivity of the exhaust, Nu_D is the Nusselt number associated with laminar flow through a tube at constant temperature, q is the heat transfer to the tube, D is the inner diameter of the tube, $c_p$is the thermal conductivity of the exhaust, and T_{lm} is the log mean temperature difference.

$$h = \frac{k_f Nu_D}{D} \qquad \text{Equation 3.1}$$

$$T_{lm} = \frac{T_{in} - T_{out}}{\log\left(\frac{T_{in}}{T_{out}}\right)} \qquad \text{Equation 3.2}$$

$$q = \dot{m} c_p (T_{in} - T_{out}) \qquad \text{Equation 3.3}$$

$$L = \frac{q}{h\pi D T_{lm}} \qquad \text{Equation 3.4}$$

It was desirable for the walls of the sample conditioner to be of uniform temperature for the length of time it takes for the sample to reach equilibrium. To keep the walls of the conditioner at a nearly uniform temperature, the greater the heat capacity and thermal mass of the conditioner, the better.

The first generation sample conditioner consisted of a stainless steel coil in an oil bath. The oil bath had a 2500W heater and a series of cooling tubes through which cooled water was run at oil temperatures below 100°C and cold air was run at oil temperatures above 100° C to prevent an explosive event due to the rapid boiling of the cooling water in oil in case the cooling tubes were to leak. The large quantity of oil took 40 minutes to heat from 20° C to 191° C and nearly four hours to cool from 191° C back down to 20° C. While it had an excellent temperature uniformity due to its high thermal mass and high heat capacity, the time it took to heat and cool the oil bath was prohibitively long. To reduce the time required for one temperature sweep, a second generation sample conditioner was designed.

The second generation conditioner was constructed out of a solid block of 6061 aluminum. Aluminum has a lower specific heat than the oil used in the oil bath and the

mass of aluminum used was about 70% that of the oil bath, resulting in 35% less energy required and therefore less time to heat and cool than the first conditioner. A 3D rendering of the designed conditioner body can be found in Figure 3.3. A fully dimensioned drawing of the conditioner can be found in Figure A1 of Appendix 5.

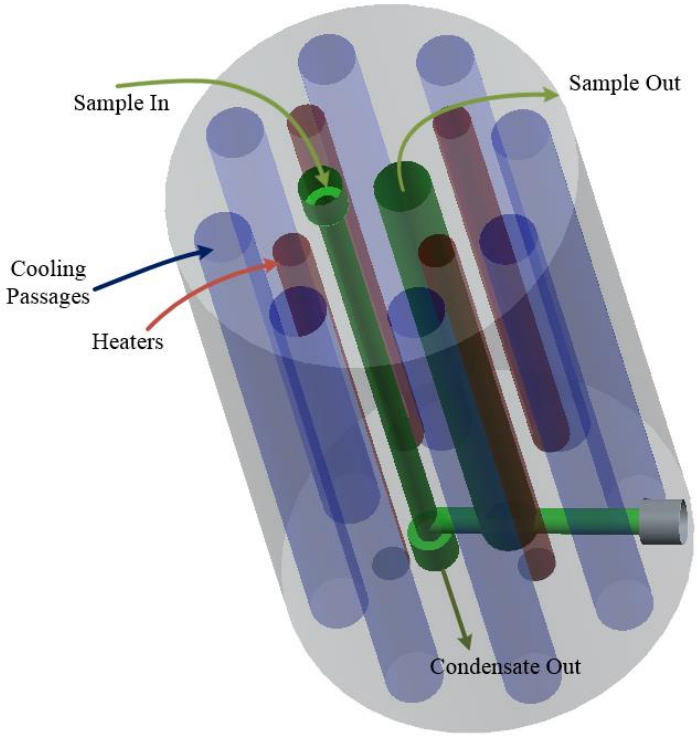

Figure 3.3: Variable temperature sample conditioner body rendering

The two center passages are the flow path for the center line and are joined by a hole drilled through the side of the conditioner that was plugged after joining the two passages. A sealed dropout was mounted to the bottom of the conditioner and kept on ice to capture the condensate collecting and running down the walls of the sample

conditioner path. Four 500W cartridge heaters were inserted into the four holes surrounding the inlet and outlet of the conditioner. Cooling water was run through the eight outlet holes on the perimeter of the block to cool the conditioner. A photo of the variable temperature sample conditioner with FIDs, sample storage, heating and cooling systems installed can be found in Figure 3.4. The VT sampling system was arranged as shown in Figure 3.5.

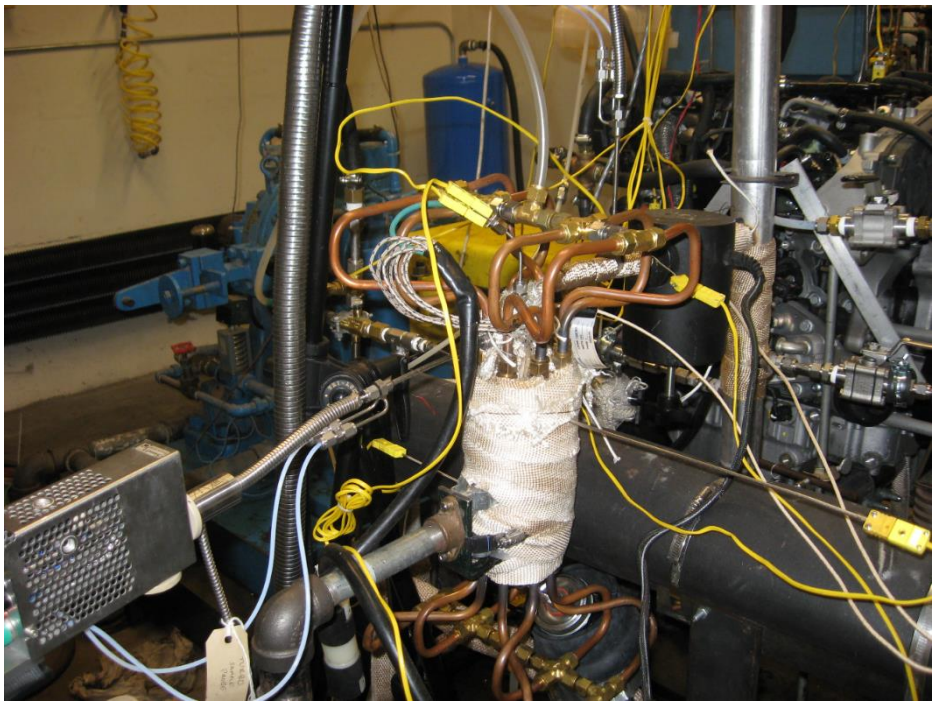

Figure 3.4: Variable temperature sample conditioner in use

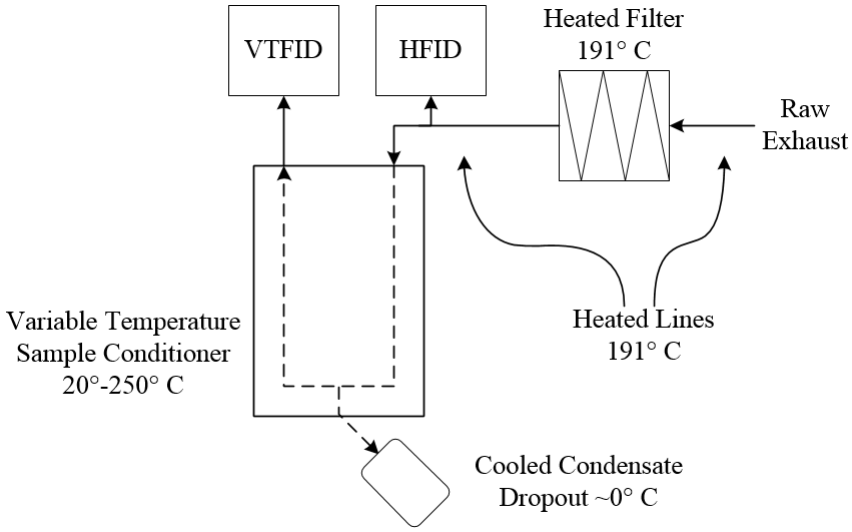

Figure 3.5: Variable temperature FID sampling setup

The sample path from the exhaust stack to the inlet of the VT sample conditioner was heated. The sample was drawn through a probe and then through a Unique Heated Products glass/PTFE filter. Downstream of the filter until of the filter the first FID channel sampled. This FID will be referred to as the hot FID (HFID). The sample then passed through a custom designed variable temperature sample conditioner before being sampled by the second FID channel. This will be referred to as the variable temperature FID (VTFID). The diameter of the sample probe for the VTFID was reduced by Cambustion to limit the flow rate to 3 L/min. The VT sample conditioner and all sample lines were insulated with fiberglass wrap and the heated VTFID probe sampled within 3 cm of the sample conditioner outlet.

Other Emissions Measurements

Additional gaseous measurements were collected using an AVL FTIR. A comprehensive list of conventional and biodiesel exhaust species measured by the FTIR can be found in Table A6 of Appendix 5. In addition to data collection of the gaseous exhaust species, the FTIR was used to set the mass percentage of EGR in the exhaust by measuring the CO_2 present in the exhaust and the CO_2 present in the intake manifold using Equation A4.1 as given by Northrop (2010) as shown in Appendix 4.

As seen in Figure 3.2 the sample lines from the exhaust, from the intake manifold and from the dilution system were connected to a heated manifold. From the manifold, the exhaust was filtered using a Unique Heated Products glass/PTFE filter. The sample line was then run through a heated line into a heated sintered stainless steel filter and into the FTIR.

Soot mass was measured using an AVL Micro Soot sensor. The Micro Soot sensor uses the photoacoustic principle to measure the mass of soot present in an exhaust sample (AVL 2013). The instrument has a built in conditioning unit that allows the user to change the ratio at which the exhaust sample is diluted. For the conditions tested, LTC exhaust was not diluted and CC exhaust was diluted 20:1. For two of the tests performed, a leak was detected in the sample conditioner. For these two tests, an ejector diluter system modeled after that used by Abdul-Khalek (1999) was used to dilute the sample before being measured by the Micro Soot sensor. The dilution ratio of the ejector diluter system was typically around 12:1 and was measured by comparing the CO_2 concentration

in the diluted exhaust using a Sable Systems CA-10A non-dispersive infrared analyzer to the CO_2 concentration in the raw exhaust using the FTIR. For the same operating condition, the soot mass measured on the day in which the dilution tunnel was used was within 6% of the soot mass measured on the day in which the AVL conditioning unit was used; indicating that two dilution systems were comparable.

3.4 Fuels

The engine was fueled with ultra-low sulfur diesel (ULSD), 100 % biodiesel (B100), as well as a 20% biodiesel-80% ULSD blend of the two fuels (B20). The B20 was splash blended to be 20% B100 and 80% ULSD by volume. When switching from ULSD to B100, the fuel system was purged and the engine run for several hours on biodiesel before taking data. The same process was used when switching from B100 to B20.

The ULSD was sent to Paragon Laboratories (Livonia, MI) to analyze its properties. The full Paragon Report can be found in Figure A2 of Appendix 5. The ULSD was also sent to Intertek (St. Rose, LA) for compositional analysis. This report can be found in Tables A1-A4 and Figure A3 of Appendix 5. The engine was also run on B20 and B100 to investigate the reduced FID response factor of oxygenated fuels.

A sample of B100 was also sent to Intertek (Romeoville, IL) to determine its fatty acid methyl ester (FAME) profile. The profile is in Table A5 of Appendix 5. A few important properties used in calculating efficiency are shown in Table 3.2. The ULSD properties shown in Table 3.2 were measured by Paragon. The B100 properties were

calculated using the measured FAME profile and the method found in Appendix 3. The properties for B20 are calculated from the B100 and ULSD listed.

Table 3.2: Fuel property comparison

	ULSD	B20	B100
LHV (MJ/kg)	42.792	42.1496	39.58
Oxygen (Wt %)	0.0%	2.192	10.96
H/C ratio	1.79	1.8	1.84

3.5 Test Procedure

Four engine operating conditions were tested to compare different HC concentrations as a function of load and combustion modes. Details of the conditions are shown in be Table 3.3. The first of two engine conditions was a 2 bar BMEP, 1500 RPM single injection ELTC condition. This condition was chosen as it was shown by Knafl, et al. (2006) to be the highest load at which ELTC was achievable. A dual injection CC mode of equivalent load and speed was developed to compare results with the corresponding ELTC mode. To achieve a higher load condition within the LTC regime, a single injection LLTC mode was developed at 4 bar 1500 RPM. The 4 bar BMEP LLTC condition was chosen as it was the highest load achievable with the stock EGR cooler. With high EGR rates, the rise in intake temperature limited the LLTC operation to 4 bar BMEP. A dual injection CC of equivalent load and speed was developed for comparison between LLTC and CC performance and emissions. Table 3.3 shows the parameters that were set for each condition tested.

Table 3.3: Engine operating parameters

Engine Condition	4 Bar BMEP LLTC	4 Bar BMEP CC	2 Bar BMEP ELTC	2 Bar BMEP CC		
Fuel Type	ULSD	ULSD	ULSD	ULSD	B100	B20
Load (Nm)	66.03	66.95	32.98	33.67	33.41	32.78
Speed (rpm)	1498	1498	1498	1498	1498	1499
Injection Pressure (Bar)	1200	750	800	500	500	500
Main Injection Timing (DBTDC)	3	10	20	7	7	7
Main Injection Duration (µs)	0.506	0.632/0.602	0.515/0.51	0.608	0.62/ 0.615	0.61/ 0.611
Pilot Injection Timing (DBTDC)	N/A	21	N/A	19	19	19
Pilot Injection Duration (µs)	N/A	.21	N/A	.21	.29	.29
Swirl Duty (%)	50	30	70	70	70	70
EGR Mass (%)	36.84	24.01	56.18	32.91	33.28	33.12
Intake Manifold Temperature (°C)	60.73	57.37	60.79	61.0	59.66	60.69

Each mode was tested on two separate days to ensure stability and demonstrate day-to-day repeatability. Four sets of data were taken on each day. There were occasional errors with the data acquisition system which prevented certain data sets from saving. For all ULSD modes tested, multiple tests on two days were saved; however, data from one

of each biodiesel test days were lost, resulting in only one day of test data for those fuels. Table 3.4 shows the total number of data sets for each condition tested.

Table 3.4: Test matrix for conditions measured

Engine Condition	4 Bar BMEP LLTC	4 Bar BMEP CC	2 Bar BMEP ELTC	2 Bar BMEP CC		
Fuel Type	ULSD	ULSD	ULSD	ULSD	B100	B20
Number of data sets	8 (4/day)	8 (4/day)	8 (4/day)	8 (4/day)	3	3

The fast FID was calibrated at least once per day using a 900 PPM propane (C3H8) and 1% CO_2 span gas and zeroed with 99.999% ultra-high purity zero grade nitrogen. On the days in which the micro-soot built in dilution system was malfunctioning and the sable CO_2 meter was used to measure dilution ratio, it was spanned with the same 1% CO_2 and 900 PPM span gas and zeroed with ultra-high purity nitrogen.

Before taking data, the engine was run at the desired operating condition for approximately 0.5 to 1 hour to allow conditions to reach steady state. A condition of steady state was determined by the following conditions: engine load and speed, intake manifold temperature and EGR rate. EGR and intake manifold temperature were simultaneously set as the mass flow rate of EGR and the temperature of the EGR affects the intake manifold temperature. The EGR mass fraction was set by measuring the CO_2 concentration in the intake manifold and the raw exhaust. The temperature of the EGR was adjusted by controlling the flow of cooling water through the EGR cooler. The intake

manifold temperature was controlled by adjusting the flow and temperature of the water through the aftercooler.

While the engine was warming up, the sample conditioner was held at 250°C to ensure that no HCs would condense in the conditioner and any hydrocarbons stored in the conditioner would be vaporized. Once the engine reached an acceptable steady state condition and the inlet and outlet HC measurements were equal, ensuring that there was no vaporization of stored components, data were taken as the sample conditioner cooled. Data were used from 191° C to the lowest temperature achieved by the conditioner. The lower temperature was usually around 18-20° C and was limited by the temperature of the tap water used to cool the conditioner. A strip chart of the sampling strategy for one testing day can be seen in Figure 3.6 showing the HCs condensing during the cooling periods and the off-gassing of stored hydrocarbons at the 250° C regeneration periods.

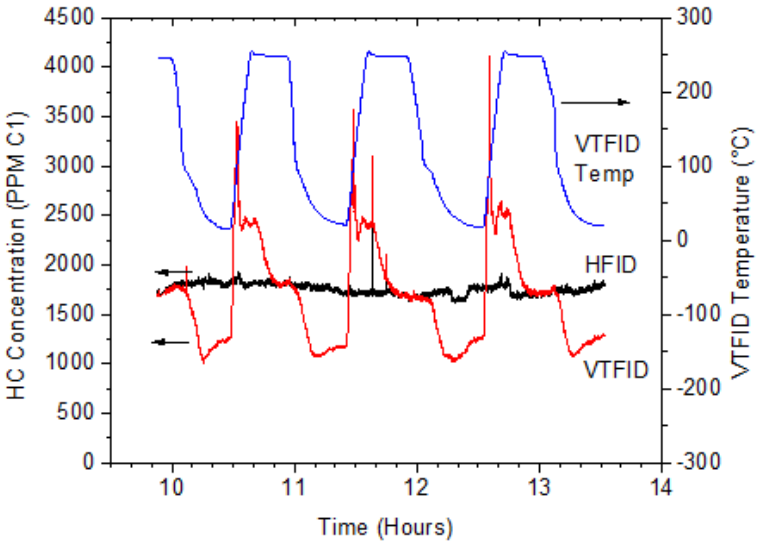

Figure 3.6: Strip chart 1500 RPM 2 bar ELTC ULSD

As the conditioner was cooled, exhaust components condensed depending on their concentration and the temperature of the sample conditioner. The condensate flowed down the walls of the conditioner and was collected in the cooled trap mounted to the bottom of the conditioner. The HFID measured the total hydrocarbons in the exhaust, the VTFID measured the remaining in the vapor phase HCs. Thus the condensable fraction of the hydrocarbons was be determined for all temperatures of the sample conditioner.

It was critical that the conditioner was continually cooled rather than warmed while data were being taken. If the conditioner was warmed- components that had condensed out of the exhaust would vaporize and be measured- misrepresenting the actual hydrocarbon quantities at the measured temperature. To ensure this would not happen, data were only taken during temperature "down sweeps" and the conditioner was regenerated between down sweeps by heating to 250° C until the VTFID and HFID reading were equal, guaranteeing no artifacts in the conditioner were being measured during the down sweep.

4 Results and discussion

4.1 GM Project Baseline Engine Results

Basic engine performance results for the four conditions can be found in Table 4.1. Appendix 1 explains the method of calculating each of the basic performance results.

Table 4.1: Basic GM engine performance results.

Engine Condition	2 Bar BMEP ELTC		2 Bar BMEP CC		4 Bar BMEP LLTC		4 Bar BMEP CC	
	Mean	Std. Dev.	Mean	Std. Dev.	Mean	Std. Dev.	Mean	Std. Dev.
Load (Nm)	33.0	0.6	33.7	0.5	66.0	0.6	66.9	1.0
Speed (rpm)	1498	2.1	1498	2.0	1498	1.1	1498	1.5
EGR Mass (%)	56.2	0.5	32.9	1.2	36.8	0.2	24.0	1.6
Intake Manifold Temp. (°C)	60.8	1.3	61.0	1.5	60.7	1.0	57.4	1.5
BSFC (g/kW-hr)	291.3	20.6	282.7	6.7	268.3	32.2	245.8	6.3
Brake Thermal Efficiency (%)	26.5	0.6	28.4	0.5	32.8	0.1	34.5	0.3
Combustion Efficiency (%)	96.2	1.8	95.0	0.5	97.3	0.2	99.3	0.04
Global AFR	19.2	2.0	40.8	6.1	18.7	0.83	25.0	3.2

The results presented in Table 4.1 demonstrate an approximately 5-7% decrease in brake thermal efficiency in a LTC mode compared to a CC mode. In both ELTC and LLTC, incomplete combustion reduces combustion efficiency and therefore reduces brake thermal efficiency as well as increases the brake specific fuel consumption (BSFC). The effect of high levels of EGR in LTC modes can be seen by the greatly reduced global air fuel ratio (AFR) in LTC compared to CC cases. The penalty in efficiency for LTC conditions is justified by the reduction in soot and NO_X as shown in the following EI plots. A detailed explanation of the calculation of EIs can be found in Appendix 2. The emissions indices for each component were calculated at each sample point. The samples were then binned together for each engine condition and averaged. The error bars on the following emissions index plots show ± 1 standard deviation.

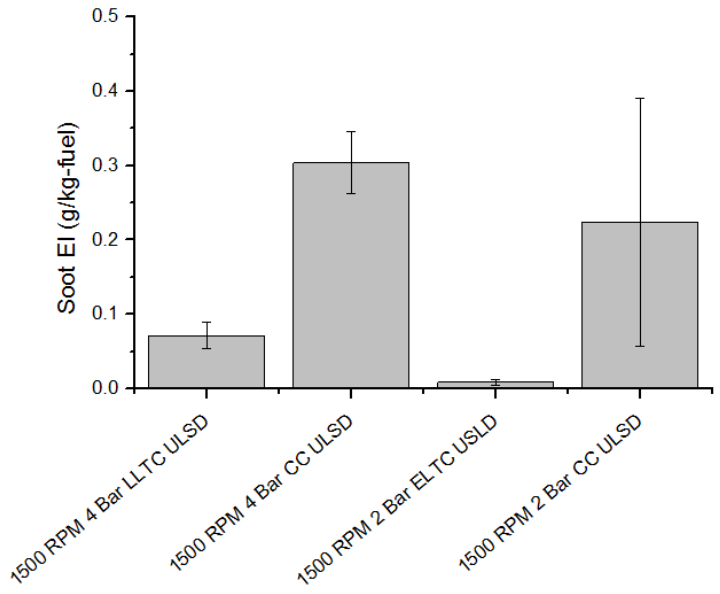

Figure 4.1: Soot mass emissions indices

As seen in Figure 4.1, the use of ELTC can practically eliminate the formation of soot due to the increased in cylinder mixing that reduces locally rich zones. LLTC also significantly reduces soot emissions standards without the use of a DPF. The large uncertainty in the 2 bar CC ULSD case is due to the soot concentration on the second test day being significantly higher than that of the first test day as the result of a creeping soot and HC condition. On the 2 bar CC ULSD operating condition, one of the test days exhibited a dramatic creeping condition in which the soot and HCs would increase drastically as demonstrated in Figure 4.2.

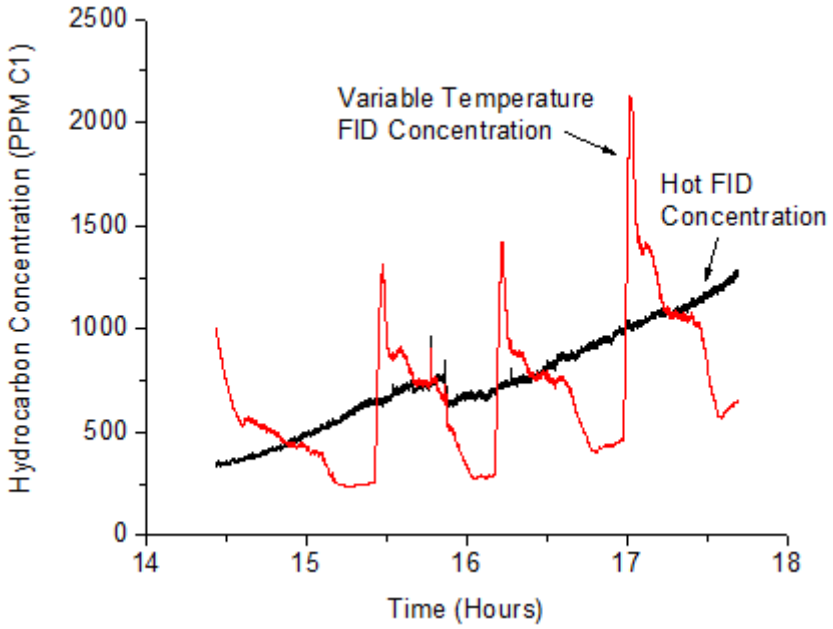

Figure 4.2: Hydrocarbon creep for 2 bar CC ULSD operating condition

During the soot and HC creep, all other engine temperatures, pressures, performance and emissions characteristics remained constant. Since the condition was ameliorated by running the engine at a high load for 15 minutes, the cause of the creep is thought to be hydrocarbon deposition on engine surfaces due to running the engine at low loads, and therefore temperatures, for extended periods of time. As these deposits become saturated, the soot and unburned hydrocarbons slowly begin to increase in the exhaust. The creep existed during the second day of testing for the 2 bar CC ULSD cases and was not noticed until after the testing was complete. All other engine performance and emissions parameters were consistent with the first test day. Lucachick, et al. (2014) show the soot EI for the 2 bar CC ULSD condition to be 0.75 g/kg-fuel. This quantity is

consistent with the first day test; the other conditions also closely match soot EI reported by Lucachick, et al. (2014).

In addition to soot, the LTC conditions also dramatically reduce NO_x due to the high levels of EGR reducing peak local temperatures as can be seen in Figure 4.3.

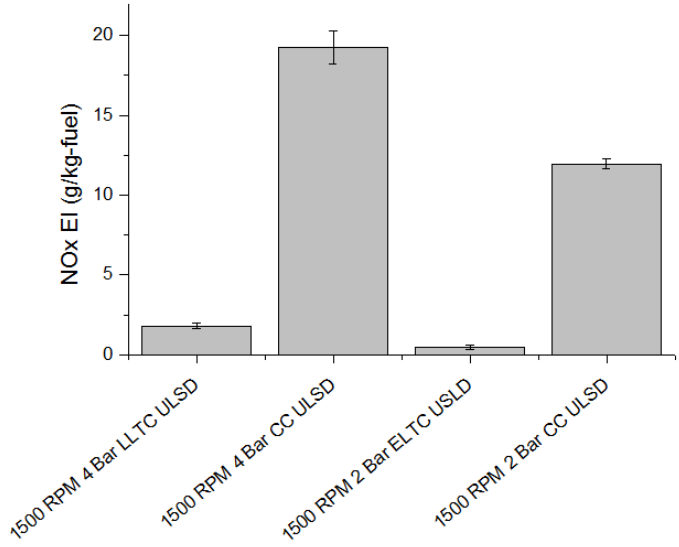

Figure 4.3: NO_X emissions indices

The ELTC mode tested practically eliminates NO_X formation and the LLTC mode reduces engine out NO_X emissions by nearly 90% for the compared to the equivalent CC mode. The higher load conventional condition has significantly higher NO_X emissions due to higher combustion temperatures.

As previously mentioned, LTC modes have lower combustion efficiencies than the CC modes and as a result, CO emissions for the LTC modes tested are significantly higher than CC modes due to incomplete combustion as seen in Figure 4.4.

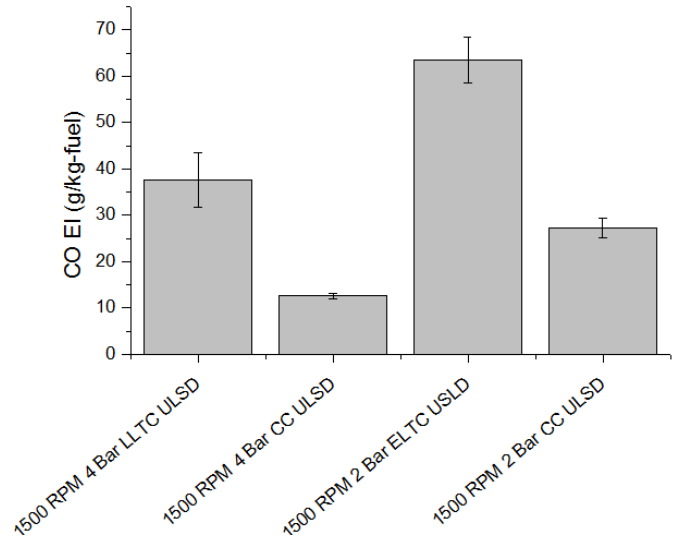

Figure 4.4: CO emissions indices

Like CO, NMOG also increase for LTC conditions due to incomplete burning as seen in Figure 4.5.

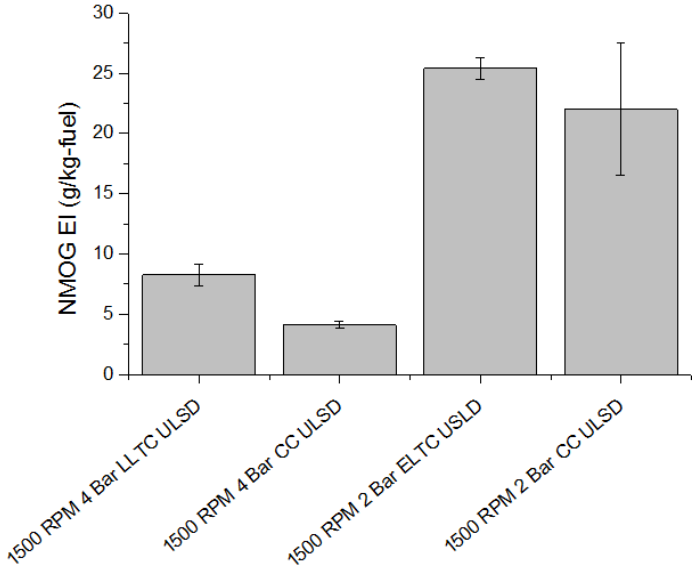

Figure 4.5: NMOG emissions indices

The higher than expected NMOG emissions and increased variation for the 2 bar CC ULSD case can be attributed to issues with hydrocarbon creep. On the first day of testing for this condition, the hydrocarbon concentration at the beginning of testing was less than 1/3 of the concentration at the end of the test as seen in Figure 4.2.

To compare the biodiesel and ULSD results, the B100 and B20 were run in engine modes similar to the ULSD CC 2 bar BMEP 1500 RPM mode. Table 4.2 shows the measured performance characteristics for the CC 2 bar BMEP 1500 RPM condition for ULSD, B100 and B20. It is evident that the performance of the biodiesel conditions are very similar to the ULSD conditions with the exception of AF ratio, and BSFC. This discrepancy is due to B100 and B20 having a lower energy density than ULSD and thus requiring more fuel to achieve the same load. The brake thermal efficiency accounts for this difference in energy density and is steady for all three conditions. The modified injection parameters used to compensate for discrepancies in energy density as well as other engine operating parameters for the biodiesel cases are shown in Table 3.3.

Table 4.2: ULSD, B100, B20 Engine performance results.

Engine Condition	2 Bar BMEP CC					
Fuel Type	ULSD		B100		B20	
	Mean	Std. Dev.	Mean	Std. Dev.	Mean	Std. Dev.
Load (Nm)	33.7	0.5	33.4	0.9	32.78	1.1
Speed (rpm)	1498	2.0	1498	2.7	1499	2.7
EGR Mass (%)	32.9	1.2	33.0	0.5	33.12	0.01
Intake Manifold Temperature (°C)	61.0	1.5	60.6	1.0	60.69	0.9
BSFC (g/kW-hr)	282.7	6.7	321.0	6.2	298.2	22.2
Brake Thermal Efficiency (%)	28.4	0.5	28.2	0.7	27.49	1.1
Combustion Efficiency (%)	95.0	0.5	94.6	0.03	95.31	2.7
Global AF ratio	40.8	6.1	34.75	0.06	36.79	0.7

4.2 Variable Temperature Hydrocarbon Ratio Data Correction

As the VT sample conditioner cooled and the dew points of different HC species were reached, HCs condensed out and the VTFID HC reading (or total HCs remaining in the vapor phase) decreased. This trend can be seen in Figure 4.6. It is expected that the VTFID concentration would monotonically decrease as the conditioner cools; however, as shown in the figure, the VTFID HC concentration increases at the end of the down sweep. This "hook" is due to an increase in VTFID HC *concentration* due to water condensing from the mixture as explained below.

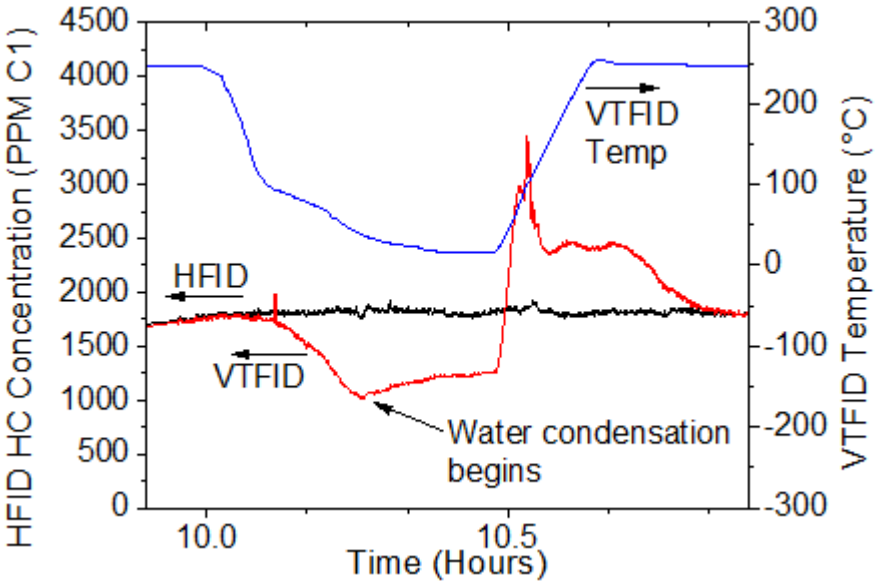

Figure 4.6: Single down sweep 1500 RPM 2 bar ELTC ULSD

Ideally, as the conditioner cools, HCs will condense out. The ratio of the difference between the HCs passing through the conditioner (VTFID) to the HCs measured at the inlet to the conditioner (HFID) is the condensed fraction at that temperature. Because the concentration of component *i* (x_i) is defined as the ratio of the moles of component *i* (n_i)

to the total moles in the mixture (n_{tot}), if the number moles of component *i* is unchanged and the total moles in the mixture is reduced, the concentration of component *i* will increase. As shown in $x_i = \frac{n_i}{n_{tot}}$ Equation 4.1.

$$x_i = \frac{n_i}{n_{tot}} \quad \text{Equation 4.1}$$

Therefore, because water vapor is a dominant component of the exhaust and is not measured by the FID, as the water begins to condense and store in the conditioner, n_{tot}, decreases and the concentration of the remaining hydrocarbons in the exhaust, n_i, increases. To correct for the change in response due to the condensing water, a correction model was created to predict the effect the condensation of water would have on the VTFID reading and the correct it depending on temperature.

To calculate the vapor pressure for water, the Antoine equation as shown in Equation 4.2 is used. Where A, B and C are Antoine's coefficients, P is the vapor pressure and T is the temperature.

$$\log_{10}(P) = A - B/(T + C) \quad \text{Equation 4.2}$$

The Antoine coefficients are empirically derived constants tabulated by several sources for a multitude of compounds. The Antoine coefficients used in this work were referenced from Yaws, Narasimhan and Gabbula (2009).

The saturation concentration of water is calculated by using the temperature at each point in the down sweep to determine the vapor pressure of water and then determining the saturation concentration by dividing the vapor pressure by the barometric pressure to get the mole fraction. If the measured water concentration by FTIR is less

than the calculated saturation concentration, no change is made. However, if the saturation concentration is lower than the measured water concentration, the difference between these concentrations is determined to be the quantity of water condensing, H_2O_{Drop}.

Besides water, the two largest components in diesel engine exhaust are CO_2 and N_2. These could also affect the FID measurement if they were to be removed. While the dew points of N_2 and CO_2 in the exhaust are much lower than attained by the sample conditioner, both N_2 and CO_2 are soluble in H_2O to some degree. Henry's law, as seen in $p_1 = K_H x_1$ Equation 4.3 is used to determine the amount of CO_2 and N_2 dissolving in the H_2O condensing within the conditioner (Battino, Rettich and Tominaga 1984).

$$p_1 = K_H x_1 \qquad \text{Equation 4.3}$$

Where p_1 is the partial pressure of N_2 or CO_2 in the exhaust, $x_1$is the mole fraction dissolved in water and K_H is Henry's law constant, a function of temperature. Henry's law constants for CO_2 were found using Equation 4.4 (Carroll, Slupsky and Mather 1991).

$$\ln\left(\frac{H_k}{MPa}\right) = -6.8346 + 1.2817 * \frac{10^4}{T} - 3.7668 * \frac{10^6}{T^2} + 2.997 * 10^8/T^3$$

Equation 4.4

Henry's law constants for N_2 were found using Equation 4.5 from Battino, Rettich, and Tominaga (1984), where τ is T(K)/100.

$$\ln(H_k) = 150.758 + 184.577\tau^{-1} + 89.599\ln(\tau) + 10.701\tau$$

Equation 4.5

The total amount of CO_2 and N_2 and H_2O dropping out (D_{CO_2,H_2O,N_2}) is determined using $D_{CO_2,H_2O,N_2} = H_2O_{Drop}\left(1 + \frac{p_{N_2}}{K_{H_{N_2}}} + \frac{p_{CO_2}}{K_{H_{CO_2}}}\right)$ Equation 4.6.

$$D_{CO_2,H_2O,N_2} = H_2O_{Drop}\left(1 + \frac{p_{N_2}}{K_{H_{N_2}}} + \frac{p_{CO_2}}{K_{H_{CO_2}}}\right)$$ Equation 4.6

Where p_{N_2} and p_{CO_2} are the partial pressure of N_2 and CO_2 in the exhaust, and $K_{H_{N_2}}$ and $K_{H_{CO_2}}$ are Henry's law coefficients for N_2 and CO_2 in the exhaust. The nitrogen concentration of the exhaust was not measured and was assumed to be 79% since that is the concentration in air and the majority of N_2 is unreacted in the combustion event. The response factor due to dilution (DRF) is found using $DRF = \frac{1000000}{1000000 - D_{CO_2,H_2O,N_2}}$ Equation 4.7. Where D_{CO_2,H_2O,N_2} is in PPM.

$$DRF = \frac{1000000}{1000000 - D_{CO_2,H_2O,N_2}}$$ Equation 4.7

It was determined that the quantities of N_2 and CO_2 removed by the condensing water were very minimal compared to the quantity of water, however they were included for completeness.

In addition to dilution effects, the readings of FIDs have been shown to be affected by the presence of water vapor (Hill and Newell 1965). Hill and Newell found that as the concentration of water vapor in the sample stream rose, the sensitivity of the FID decreased. A curve was fit to the data given by Hill and Newell to determine the

water response correction factor, WCF, as a function of water concentration in the exhaust as seen in $WRCF = 1.05{H_2O_{PPM}}^{-.0339}$ Equation 4.8. Where H_2O_{PPM} is the lower of the calculated saturation concentration or the measured concentration of water in PPM.

$$WRCF = 1.05{H_2O_{PPM}}^{-.0339} \quad \text{Equation 4.8}$$

The total correction applied to the raw VTFID data is the product of WRCF and DRF. The WCRF is also applied to the HFID data using the measured concentration of water in the exhaust.

Due to the HC creep condition previously described and the slight variability in engine HC emissions for the tested conditions, down sweeps were normalized by dividing the VTFID reading by the HFID reading to show the fraction of HCs remaining in the vapor phase. The following HC ratio results are reported and calculated by the following:

$$HC\ Ratio = \frac{HC_{VTFID}[PPM]}{HC_{HFID}[PPM]} \quad \text{Equation 4.9}$$

The raw HC ratio and corrected HC ratio down sweeps taken from the 4 bar LLTC case are shown in Figure 4.7.

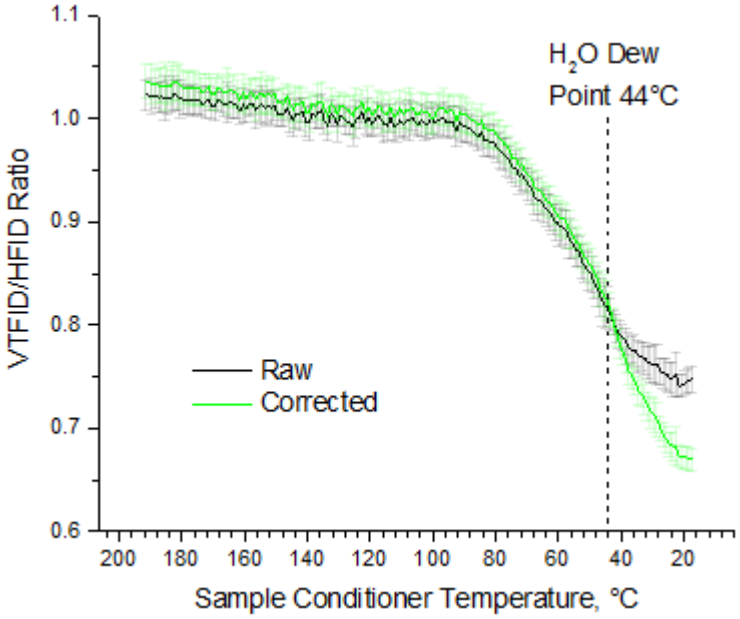

Figure 4.7: 4 bar LLTC raw ratio of measured HC concentrations during a temperature down sweep

As shown in the raw data curve of Figure 4.7, there is a kink in the curve at the dew point of water when the water in the exhaust begins to condense. By applying the aforementioned corrections, the corrected data curve is created and the dramatic change in slope at the dew point of water is eliminated.

To test the robustness of the model and to check that hydrocarbons would condense out in the conditioner as expected, the sample conditioner was run with the FTIR measuring the outlet of the sample conditioner.

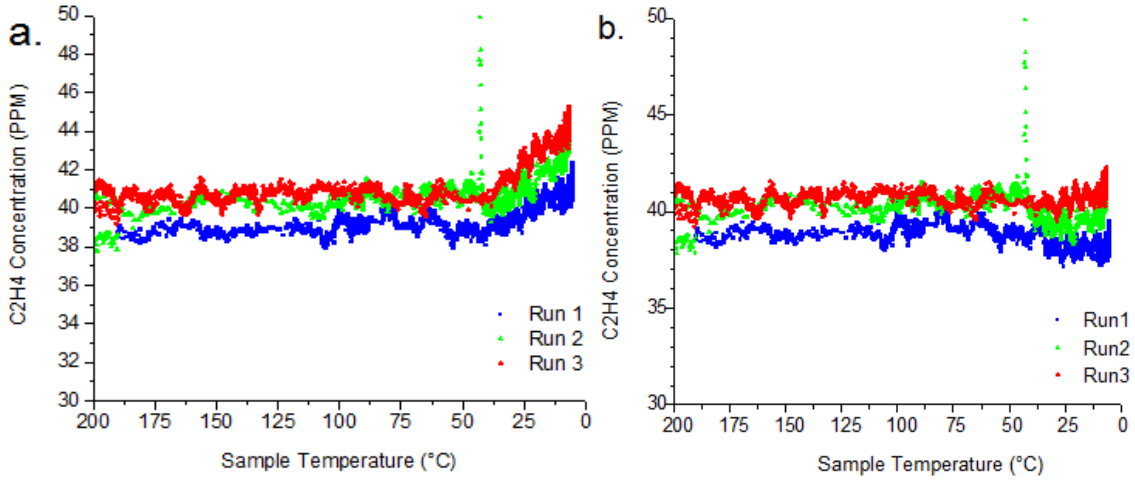

Figure 4.8: FTIR measurement on outlet of variable temperature sample conditioner for 2 bar CC ULSD operation a. Raw C_2H_4 measurement b. C_2H_4 measurement corrected with model

As seen in Figure 4.8a., over a range of temperatures, the light HCs do not condense out and as soon as water starts to condense, the removal of the diluent artificially increases the hydrocarbon concentration. With the model described above, the artificial hook is removed as shown in Figure 4.8b. Figure 4.9 shows the effect of the sample conditioner on octane (NC8) as measured by the FTIR.

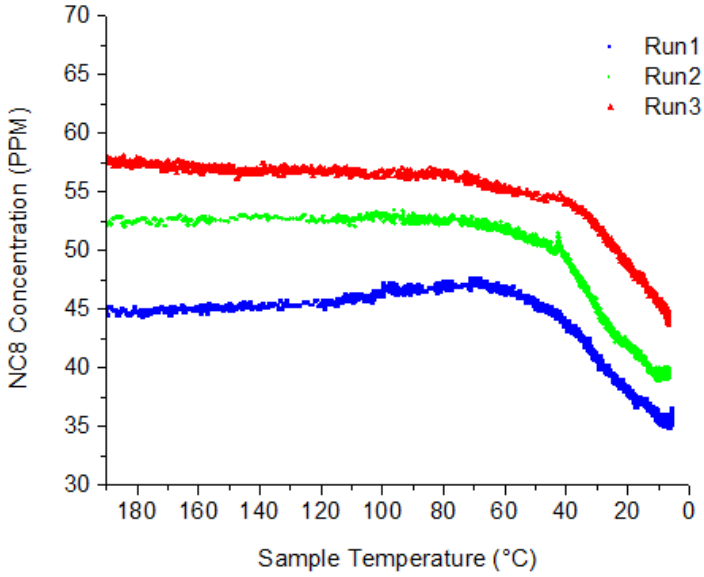

Figure 4.9: FTIR NC8 measurement on outlet of variable temperature sample conditioner for 2 bar CC ULSD operation

Figure 4.9 demonstrates a heavier HC condensing out as the sample conditioner cools. Figure 4.8 and Figure 4.9 also demonstrate that the effect of hydrocarbon creep is present across a range of hydrocarbon molecular weights as each run is progressively higher for both the light hydrocarbons and the heavy; however more pronounced for the heavy HCs further confirming that the creep is due to a condensation, saturation and re-evaporation storage scheme within the engine.

4.3 ULSD Variable Temperature Sample Conditioner Results

The data correction was applied to all of the down sweeps. For each condition, all of the down sweep ratios were combined into a single data set and then binned into 1 degree increments. In each 1 degree bin, the data was averaged and plotted in the following figures. The error bars on the down sweep plots presented represent ±1

standard deviation. Data are plotted with a decreasing x-axis to demonstrate a cooling down sweep from left to right. When analyzing the reported down sweeps, it is important to recall that the sweeps are normalized to the HFID condition to compensate for variation in sweep to sweep absolute hydrocarbon concentrations. That is, the results show the fraction of the total, not the absolute amount of hydrocarbons condensing.

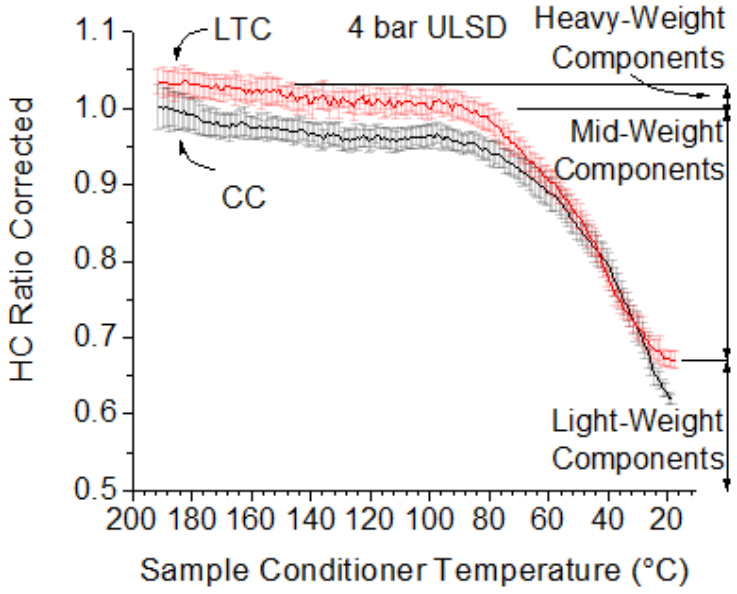

Figure 4.10: 4 bar ULSD CC and LLTC down sweeps

Figure 4.10 shows the CC and LTC down sweeps for the 4 bar ULSD conditions. The typical down sweep can be broken into three separate regions, the heavy weight components that condense at the highest temperatures, the middle weight components that condense at moderate temperatures and the light components that are not removed at the temperatures used in this study. As first discussed in Andrews (2000), the dependence of FID-measured HC on temperature can be used for a quantitative measurement of the fractions of HC. It is proposed that the heavy weight components condensing out at the

highest temperatures are due to lubricating oil present in the exhaust as this is the heaviest hydrocarbon species introduced into the engine. The mid-weight components are proposed to be unburned fuel (further discussed in the following biodiesel section) and the light components are proposed to be partially burned fuel that is too light to condense over the range of temperature swept by the VT sample conditioner. The cutoff between heavy-weight and medium weight components was defined by the point at which the rapid hydrocarbon condensation began, that is, the "knee" where the HC ratio curve sharply transitions to its steepest slope.

Because the down sweeps are taken as a ratio, the fraction of the total heavy weight components in Figure 4.10 is much higher in the CC case than the LTC case. Since the absolute concentration of hydrocarbons in the exhaust of the LTC case is more than double that of the CC case, the reduced fraction of heavy HCs indicates that the fraction of heaviest components does not increase with the overall concentration. This is consistent with the hypothesis that the heaviest components are due to lube oil as the lube oil fraction would remain relatively constant for a given engine load and speed regardless of combustion mode.

The convex "tail" of the LTC curve indicates that if the conditioner were capable of cooling to a lower temperature, the ratio would approach an asymptotic value, and fraction of hydrocarbons below this asymptote would be the light hydrocarbons that do not condense in the temperature sample range. The CC curve closely matches the upper half of the LTC curve, and, over the range of temperatures tested, does not begin to

approach an asymptotic value like the LTC curve suggesting that if the conditioner were to continue to cool, a higher fraction of HCs would continue to condense. Because the CC curve is continuing to drop below a HC ratio of 0.6 and the LTC curve is leveling out near 0.67, this indicates that 67% of the hydrocarbons in the LTC exhaust is due to partially burned fuel while less than 60% is partially burned in the CC case. Since light hydrocarbons are formed from incomplete combustion, the higher fraction in LTC exhaust is consistent with what would be expected (Dec 2009) (Musculus, et al. 2007).

In theory, the ratio of VTFID hydrocarbons to HFID hydrocarbons should be 1 at 191° C. However, the ratio for the 4 bar ULSD LTC condition is slightly above 1. During data collection, the decision to begin a down sweep was made when the VTFID and HFID readings were equal. Due to the variability of the readings during testing, a few down sweeps for the 4 bar ULSD case were initiated with the actual VTFID reading being slightly higher than the HFID reading affecting the VTFID concentrations at the highest temperatures sampled. This effect does not propagate throughout the rest of the down sweep as HCs begin to condense.

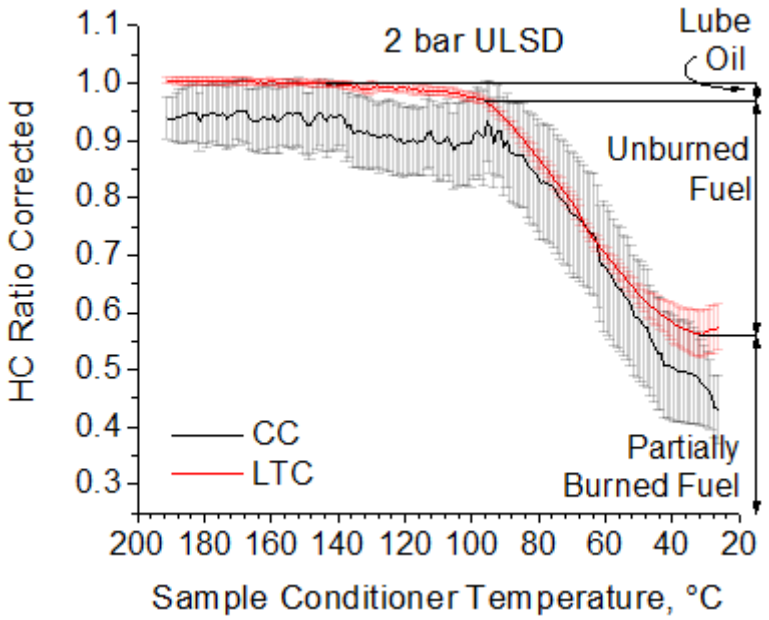

Figure 4.11: 2 Bar ULSD ELTC and CC down sweeps

The CC and LTC curves for the ULSD 2 bar conditions are shown in Figure 4.11. The shape of the curves for the 2 bar conditions follow similar shapes to the 4 bar conditions with a much larger fraction of hydrocarbons condensing in the 2 bar CC case. This is reasonable because the absolute HC concentrations in the exhaust for the 2 bar CC case are nearly 3 times the absolute concentrations in the 4 bar CC case resulting in higher saturation temperatures. This trend supports the idea that the majority of hydrocarbons in the exhaust for the CC conditions are medium weight hydrocarbons, or unburned fuel since the ratio is continuing to fall below 0.45 without showing signs of reaching an asymptotic value; indicating greater than 50% of the hydrocarbons in the exhaust are due to unburned fuel. The large uncertainty in the CC case is due to the hydrocarbon creep previously mentioned that plagued the 2 bar CC condition.

Just as in the 4 bar LTC case, the much higher absolute concentrations of HC in the exhaust suppresses the heavy fraction in the ratio versus temperature curve seen for the LTC case. The asymptotic indicator for light HCs is much clearer for the 2 bar case and indicates that the partially burned fuel accounts for approximately 56% of the hydrocarbons in the exhaust with 44% accounting for unburned fuel.

4.4 Biodiesel Variable Temperature Sample Conditioner Results

The 2 bar CC condition was also tested using B20 and B100. The same correction model used for ULSD was applied to both down sweeps and the curves are shown in Figure 4.12.

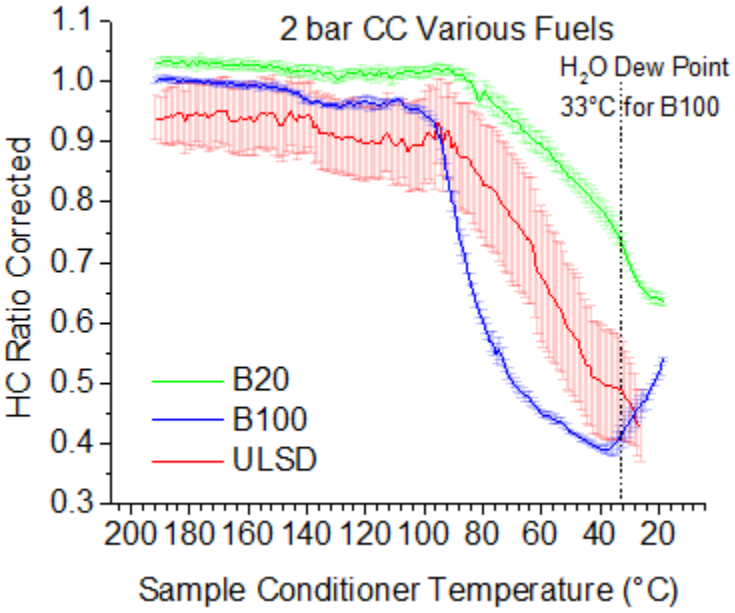

Figure 4.12: 2 Bar CC biodiesel down sweeps

The B20 curve has a similar to shape to the ULSD curve but the fewer absolute hydrocarbons in the exhaust for the B20 case results in a lower condensed fraction in the

temperature range tested. In addition, the lower absolute HC concentration results in a lower HC dew point, pushing the "knee" or the start of unburned fuel condensation to a cooler temperature. There is also a distinct change in the slope of the dropout curve near 33º C that could be attributed to the fraction of unburned biodiesel in the exhaust dropping out. The curve also seems to approach an asymptote similar to the LTC curves for ULSD. This could be the case, but it is more likely that the reduced response factor for oxygenated compounds underestimates the total HFID hydrocarbon reading so as the biodiesel begins to drop out, the reported fraction of hydrocarbons that have not condensed is higher than the actual remaining fraction as further demonstrated in the B100 results.

The B100 curve was corrected using the same model as the ULSD cases to compensate for water, N_2, and CO_2 drop as well as response factor in the presence of water; however, it exhibits a steep hook near the dew point of water even after the correction model is applied. This hook is in part, the result of the reduced response factor for oxygenated HCs. This reduced sensitivity is reported as a response factor. For example, if the response factor for a component is 0.5, the FID only reports 50% of the actual concentration present. For most non-oxygenated hydrocarbons FID response factors are nearly 1; however, for fatty acid methyl esters FID response factors can be as low as 0.2 (Dietz 1966). Therefore, if the exhaust contains a high concentration of hydrocarbons with a low response factor, the total hydrocarbon concentration (HFID) would be underestimated. If these low response hydrocarbons then begin to condense, the

effective response factor of the remaining hydrocarbons will increase due to the loss of low reactivity components. As the response factor for the remaining portion increases, the total response factor for the HFID measurement will remain constant resulting in an artificial increase in the fraction of remaining hydrocarbons thus the hook on the down sweep for the B100 case would be exacerbated due to the reduced response to oxygenated compounds.

Figure 4.13 shows a detailed strip chart of the B100 test day.

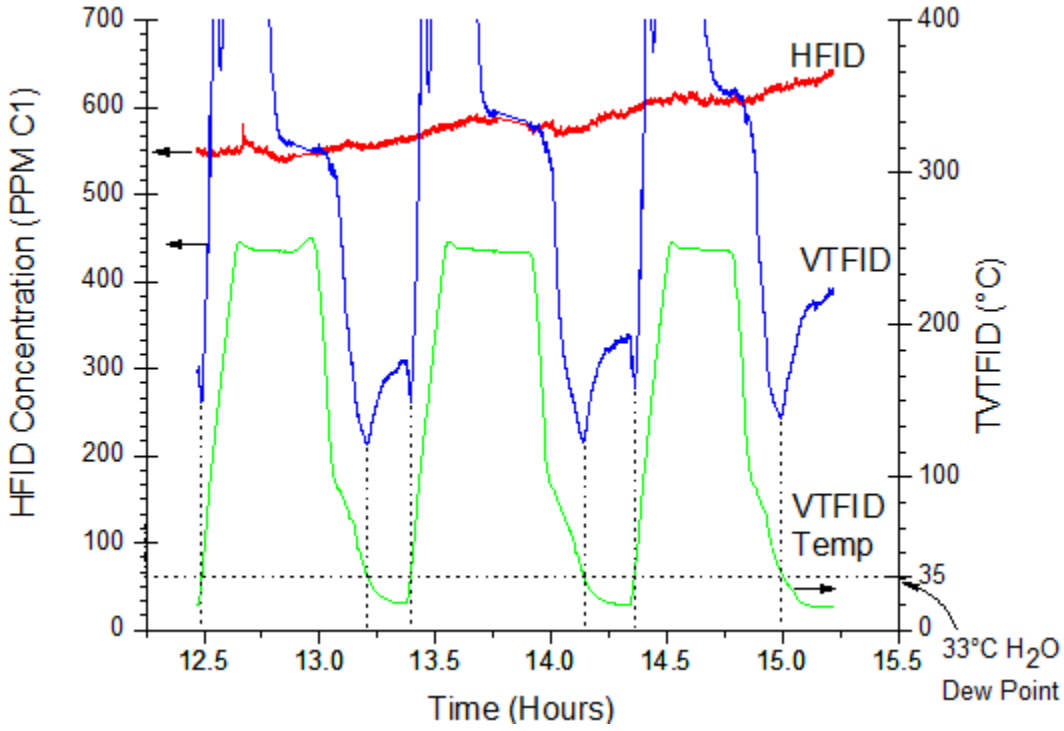

Figure 4.13: Detailed strip chart for the 2 bar B100 CC condition

The strip chart shows the effect of temperature on absolute hydrocarbon concentration, not a normalized basis. As the conditioner cools, the VTFID concentration decreases as expected until near the dew point where water begins to condense.

The VTFID concentration then increases as the water condenses due to the previously explained loss of a diluent. Once the temperature of the sample conditioner has reached its coolest setting, the down sweep is complete and the heaters are turned back on to regenerate the sample conditioner. In all of the sample conditions except for the 2 bar B100 CC case when the sample conditioner is heated after the down sweep, the VTFID hydrocarbon concentration immediately spikes (see Figure 3.6) as the hydrocarbons that have condensed and been stored on the walls begin to evaporate. The B100 case is unique in that upon heating, the sample conditioner after the down sweep, the concentration decreases until 35 °C upon which it follows the same peaking trend as the other conditions. This decrease on heating is due to the sample being diluted by evaporating water. It is important to note that between the minimum and 35 °C water is evaporating but no hydrocarbons are evaporating until 35 °C. This indicates that below 35° C, no more hydrocarbons are condensing than at 35 °C demonstrating a clear boundary between middle weight and light weight components and indicating that at 35 ºC, all of the middle weight HCs (unburned fuel) have been removed from the exhaust.

4.5 Estimation of Effective Total HC Response Factor for Biodiesel Operation

98% of the biodiesel tested was composed of only five different esters, and just two esters account for 75% of the fuel. All five esters are of similar composition as shown in Table 4.3. As a result, the range of temperatures at which the unburned esters condense out is extremely narrow; hence the extremely steep down sweep curve for B100 in Figure 4.1. In addition to condensing rapidly, the clear boundary between middle

weight and light weight components demonstrated by the 35 °C minima indicate that all of the hydrocarbons attributed to unburned fuel have condensed by 35 °C and only the partially burned hydrocarbons remain.

Using the knowledge that no more hydrocarbons are condensing out at or below 35 °C, it is assumed that all of the hydrocarbons dropping out in the steepest region of the down sweep before 35 °C are composed of unburned B100. A model was constructed using the fatty acid profile of B100. To simplify the model, the fuel was assumed to be made up of the 5 major components. The mole fractions (normalized to 5 components) of each component can be found in Table 4.3:

Table 4.3: Makeup of B100 normalized to 5 components

	C16:0	C18:0	C18:1N9T	C18:2N6T	C18:3N6
Molecular Formula	$C_{17}H_{34}O_2$	$C_{19}H_{38}O_2$	$C_{19}H_{36}O_2$	$C_{19}H_{34}O_2$	$C_{19}H_{32}O_2$
Raw Mole Percent	11.04	5.03	25.03	50.41	7.28
Normalized Mole Percent	11.18	5.09	25.34	51.02	7.37

The concentration of each of the species in the exhaust (x_{i_e}) was determined by converting the normalized mole fraction to a mole fraction on a C1 basis ($x_{i_{C_1}}$) and multiplying this fraction by the total hydrocarbons in the exhaust and converting back to a carbon weight basis using Equation 4.10 where x_{i_f} is the mole fraction of component *i* in the fuel, n_{C_i} is the carbon number of component *i*, and THC_{PPM} is the total concentration of hydrocarbons in the exhaust on a C1 basis as measured by the hot FID.

$$x_{i_e} = \frac{\frac{x_{i_f}}{\sum x_{i_f} n_{C_i}} THC_{PPM}}{1000000}$$

Equation 4.10

The saturation concentration for each component is calculated using the Antoine Equation ($\log_{10}(P) = A - B/(T + C)$ Equation 4.2) and Antoine constants for each component as given in Yuan, Hansen, and Zhang (2005). The saturation concentration is calculated for each component at the range of temperatures swept by the sample conditioner. At each temperature, the saturation concentration is compared to the initial concentration of each component in the exhaust and the lower of the two taken to be the concentration at that temperature. The concentration of each component is then converted to a C1 basis and totaled to determine the concentration of total hydrocarbons in the exhaust at each temperature. An example of the modeled condensation curve for an initial concentration of 1000PPM and an initial concentration of 460 PPM fuel in the exhaust at a barometric pressure of 98.52 kPa is shown in Figure 4.14.

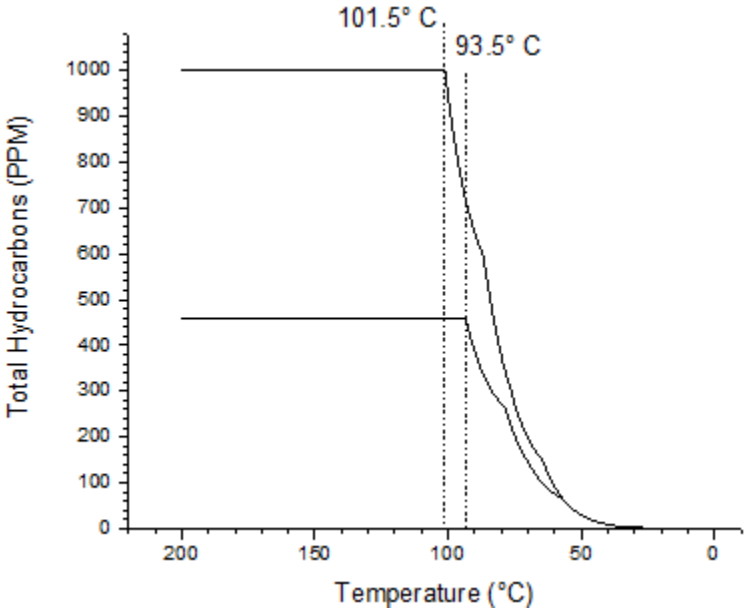

Figure 4.14: Sample model-produced condensation curves for B100 at two initial total HC concentrations, 460 ppm and 1000 ppm

The shape of the curve pictured in Figure 4.14 is similar to the B100 Curve depicted in Figure 4.12. The knee in the model clearly shows the B100 dew point, that is, the temperature at which B100 begins to condense. As the initial concentration of the exhaust increases, the temperature at which condensation begins also increases. By comparing the exhaust B100 dew point determined by the data to the B100 dew point determined by the model, an estimate for the actual concentration of unburned fuel in the exhaust can be determined. Figure 4.14 shows the heavy, mid weight, and light weight hydrocarbon regions defined as well as the B100 dew point, defined as the temperature where the transition to the steepest descent at which the mid weight hydrocarbons begin to condense occurs, 93.5° C.

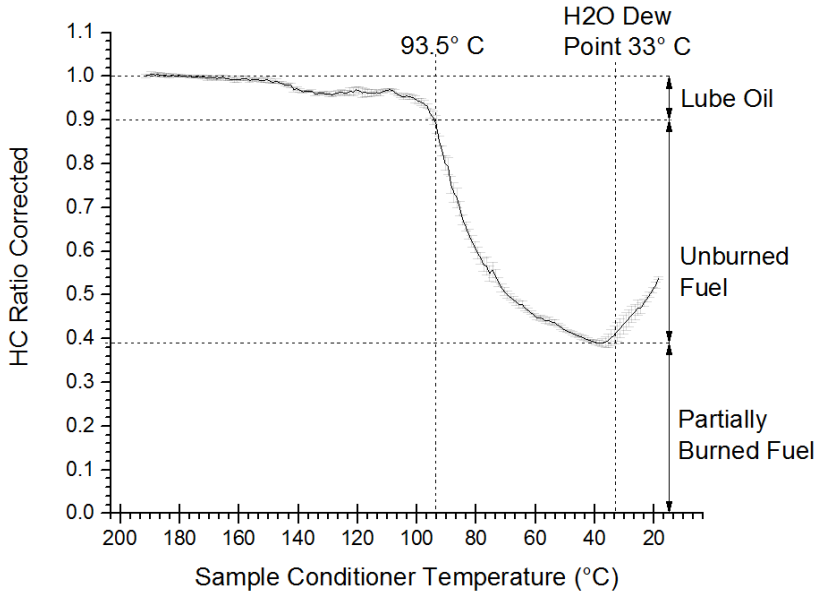

Figure 4.15: 2 Bar B100 CC exhaust hydrocarbon distribution

Using the condensation model, it was determined that for the knee to occur at 93.5° C, the initial concentration of unburned fuel in the exhaust must be 460 PPM as seen in Figure 4.14. The total HC reading (HFID) from the exhaust is 582 PPM, 51% of which, as shown by Figure 4.15, is considered to be unburned fuel. Therefore the theoretical response factor determined for the unburned biodiesel is 0.65 resulting in a response factor of 0.77 for the total HC in the exhaust using the FID tested.

To see the effect of the theoretical response factor on the exaggerated hook, the fraction of hydrocarbons in the "unburned" fuel portion of the condensation curve were divided by the theoretical response factor of 0.65 and plotted in Figure 4.16. The response factor for the lube oil portion and the partially burned fuel fraction were determined to be 1. Also shown in Figure 4.16 is the model for 460 ppm unburned fuel

which has been normalized to a ratio using the partially burned and lube oil portion from the data as defined by Figure 4.15.

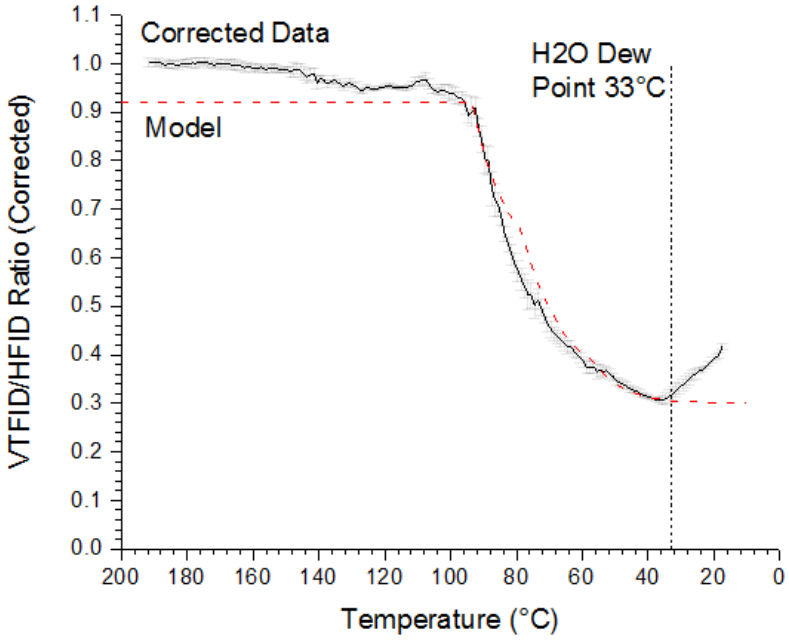

Figure 4.16: Response factor 0.653 corrected 2 bar B100 CC and model

The model and corrected data match quite well until the dew point of water where there is still a hook on the data. The remaining hook could be due in part to the slight temperature gradient that exists in the conditioner at the lower temperatures. If the temperature is colder than reported, the condensing water will be underestimated. Also, the data given by Hill and Newell (1965) used to create the correction response factor due to the presence of water is limited. It would be beneficial to measure the response factor due to water concentration for this system to determine the accuracy and applicability of the Hill and Newell data. It would also be desirable to run more repeat test days and the steadier 4 bar load condition to validate the response factor estimation method and

confirm the existence and magnitude of the remaining hook. Even with the remaining inconsistencies in the light HC region, middle weight hydrocarbons match the theoretical model of condensation quite well, validating the assumption that the middle weight hydrocarbons are unburned fuel.

Because the reduced FID response of oxygenated species depends on competing chemical reactions, it is difficult to theoretically calculate FID response factors for individual instruments. Schreiner et al. (2004) and others have discussed a theory used to estimate the response factor of FAMEs that operates under the carbon deficiency method. As FID response is proportional to the number of carbons in the measured molecule, the theory estimates that the response of a FAME will be reduced by a 1.5 carbons due to the carbonyl group not being detected and the alcohol group being partially detected. According to this theory, the theoretical measured response factor for C18:0, a major component of the B100 tested, normalized to $C_{20}H_{42}$ is 0.83 and the measured response factor is 0.82. This response factor is inconsistent with the response factor determined here by the condensation model; however, the theoretical response factors determined by this theory are also inconsistent empirical response factors reported by Dietz (1966) and others.

It has been shown by Badings and De Jong (1983) that response factors are instrument and system dependent; in addition, EPA regulations recommend determining response factors for individual FIDs with an alcohol/carbonyl calibration gas (US EPA 2010). Because response factors depend on competing chemical reactions, and therefore

environmental variables, it is best to determine response factors on an independent system basis. Thus, in order to determine the quality of the response factor measured using the VT sample conditioner and condensation model; this method must be evaluated by measuring oxygenated calibration gases or by evaporating liquid substances with known concentrations.

5 Conclusions and Recommendations

5.1 Summary and Conclusions

A custom designed variable temperature sample conditioner was developed and tested with two fast-response FIDs was used to determine the condensable fraction of hydrocarbons present in engine exhaust over a range of temperatures. A correction model was used to compensate for water condensing from the exhaust, nitrogen and carbon dioxide dissolving in the condensing water and the reduced response factor of a FID in the presence of water. The sample conditioner along with the correction model were used to estimate the distribution of lube oil, partially burned, and unburned hydrocarbons in diesel exhaust.

A modern light-duty diesel engine was run at four engine operating conditions. Two separate loads, two combustion strategies, and three fuels were examined using the sample conditioner and correction method. It was estimated that in a 1500 RPM, 2 bar ULSD LTC case approximately 56% of the hydrocarbons are partially burned fuel and 44% are unburned fuel whereas in a 1500 RPM 2 bar ULSD CC case was made up of greater than 55% unburned fuel. A1500 RPM 4 bar ULSD LTC case was estimated to be

made up of approximately 67% partially burned fuel and 31% unburned fuel while a 1500 RPM 4 bar ULSD CC case was greater than 35% unburned fuel.

A theoretical model predicting the condensation of unburned biodiesel was created using Antoine's equation and was used to validate the assumption that the middle weight condensing hydrocarbons were unburned fuel. The model was also used to estimate the relative response factor of 0.65 for the unburned biodiesel resulting in a response factor of 0.77 for the total HC in the exhaust using the FID tested. The demonstration of this concept provides a basis for future research into its application to further identify components in diesel engine exhaust and determine the effective FID response factor for oxygenated fuels.

5.2 Future Recommendations

The work described here demonstrates a proof of concept and a baseline evaluation of the variable temperature sample conditioner condensation method. To further improve the accuracy of the approach and validate the measurements of the method, further work must be completed.

To accurately identify the quantity of unburned ULSD in conventional combustion, a sample conditioner with capabilities of reaching colder temperatures is necessary. In addition, to avoid the temperature gradient at lower temperatures a conditioner with more even temperature distribution would be ideal. A conditioner capable of rapidly heating and cooling a large thermal mass such as an oil bath with circulation is recommended as it would increase sample acquisition speed.

It would also be beneficial to test a wider range of loads and combustion strategies with B100 such as the 2 bar BMEP LTC condition and both the LTC and CC 4 bar conditions to determine the robustness of the biodiesel response factor prediction. In addition, the biodiesel response factor estimation approach should be validated by measuring a known concentration of vaporized biodiesel or using a high enough concentration FAME calibration gas in this system. The VT conditioner could also be used to evaluate Hill and Newell's effect of water content on FID response. Finally it would be ideal to verify the estimations of the three HC groups through the use of GC analysis.

References

Abdul-Khalek, Imad Said. 1999. "Influence of Dilution Conditions on Diesel Exhaust Nanoparticle Emissions: Experimental Investigation and Theoretical Assessment." PhD Thesis.

Air Resources Board. 2012. *California Non-Methane Organic Gas Test Procedures.* Test Procedure, El Monte: California Environmental Protection Agency.

Akihama, Kazuhiro, Toshiki Takatori, and Kasuhisa Inagaki. 2001. *Mechanism of the Smokeless Rich Diesel Combustion by Reducing Temperature.* Technical Paper, Detroit: SAE International.

Andrews, G.E., M.K. Abbass, A. Abdelhalim, J. Farrar-Khan, M., Ounzain, A. Ghazikhani, F.M. Salih, and Y. Shen. 2000. *Unburned Liquid Hydrocarbons Using Differential Temperature Hydrocarbon Analysers.* Technical Paper, Detroit: SAE International.

AVL. 2013. *AVL Micro Soot Sensor.* Accessed 1 10, 2014. https://www.avl.com/micro-soot-sensor.

AVL. 2013. *SESAM i60 FT Multi Component Exhaust Measurement System.* Accessed 2 5, 2014. https://www.avl.com/sesam-i60-ft.

Badings, H.T., and C. De Jong. 1983. "Glass capillary gas chromatography of fatty acid mthyl esters. A study of conditions for the quantitative analysis of short- and long-chain fatty acids in lipids." *Jounal of Chromatography* 493-506.

Bart, Jan C. J., Natale Palmeri, and Stefano Cavallaro. 2010. *Biodiesel Science and Technology - From Soil to Oil.* Boca Raton, FL: Woodhead.

Battino, Rubin, Timothy R. Rettich, and Toshihiro Tominaga. 1984. "The Solubility of Nitrogen and Air in Liquids." *Journal of Physical Chemistry* 563-600.

Blumberg, Leonid M. 2012. "Theory of Gas Chromatography." In *Gas Chromatography*, by Colin Poole, 19-78. Oxford, UK: Elsevier.

Calcote, H.F. 1961. "Ion production and recombination in flames." *International Symposium on Combustion* 184-199.

Cambustion. 2014. *HFR500 hydrocarbon analyzer.* Accessed 1 10, 2014. http://www.cambustion.com/products/hfr500.

Carroll, John J., John D. Slupsky, and Alan E. Mather. 1991. "The Solubility of Carbon Dioxide in Water at Low Pressure." *Journal of Physical Chemistry Reference Data* 1201-1209.

Cheng, Wai K., Tim Summers, and Nick Collings. 1998. "The fast-response flame ionization detector." *Progress in Energy and Combustion Science* 89-124.

Dec, John E. 2009. "Advanced compression-ignition engines- understanding the in-cylinder processes." *Proceedings of the Combustion Institute* 2727-2742.

Dietz, W.A. 1966. "Response Factors for Gas Chromatographic Analyses." *Journal of Gas Chromatography.*

Franklin, Luke. 2010. "Effects of Homogeneous Charge Compression Ignition (HCCI) Control Strategies on Particulate Emissions of Ethanol Fuel." PhD Thesis.

Greeves, G., I. Khan, and C., Fenne, I. Wang. 1977. "Origins of Hydrocarbon Emissions from Diesel Engines." *SAE International.*

Heywood, John B. 1988. *Internal Combustion Engine Fundamentals.* New York: McGraw-Hill.

Hill, D.W., and H.A. Newell. 1965. "Effect of Water Vapour on the Sensitivity of a Flame Ionization Detector for Gas Chromatography." *Nature* 708-709.

Hill, Jason, Erik Nelson, David Tilman, Stephen Polasky, and Douglas Tiffany. 2006. "Environmental, economic, and energetic costs and benefits of biodiesel and ethanol biofuels." *Proceedings of the National Academy of Sciences of the United States of America* 11206-11210.

Holm, Torkil. 1999. "Aspects of the mechanism of the flame ionization detector." *Journal of Chromatography A* 221-227.

Johnson, Timothy. 2013. "Vehicular Emissions in Review." *SAE International.*

Kamimoto, Takeyuki, and Myurng-hoan Bae. 1988. "High Combustion Temperature for the Reduction of Particulate in Diesel Engines." *SAE Technical Paper.*

Kashdan, Julian T., Sylvain Mendez, and Bruneaux Gilles. 2007. "On the origin of Unburned Hydrocarbon Emissions in a Wall Guided, Low NOx Diesel Combustion System." *SAE International* 744-767.

Knafl, A., T. Jacobs, S.V. Bohac, and D.N. Assanis. 2006. "The Load Limits of Low Temperature Premixed Compression Ignition Diesel Combustion." *The Second*

International Symposium on Clean and High-Efficiency Combustion in Engines. Tianjin, China. 49-56.

Koci, Chad P., Youngchul Ra, Roger Krieger, Mike Andrie, David E. Foster, Robert M. Siewert, Russell P. Durrett, Isaac Ekoto, and Paul C. Miles. 2009. "Detailed Unburned Hydrocarbon Investigations in a Highly-Dilute Diesel Low Temperature Combustion Regime." *SAE International* 858-879.

Larson, Eric D. 2008. "Biofuel production technologies: status, prospects and implications for trade and development." *United Nations Conference on Trade and Development.* New York and Geneva: United Nations.

Lewis, Samuel A., John M. E. Storey, and Bruce Bunting. 2005. "Partial Oxidation Products and Other Hydrocarbon Species in Diesel HCCI Exhaust." *SAE International.*

Lucachick, Glenn, Aaron Avenido, William Northrop, and David Kittelson. 2014. "Exploration of Semi-Volatile Particulate Matter Emissions from Low Temperature Combustion in a Light-Duty Diesel Engine." *SAE International.*

Martyr, A. J., and M. A. Plint. 2012. *Engine Testing.* Oxford, UK: Elsevier.

McCormick, R.L., A. Williams, J. Ireland, M. Brimhall, and R.R. Hayes. 2006. *Effects of Biodiesel Blends on Vehicle Emissions.* Milestone Report, Golden: National Renewable Energy Laboratory.

McWilliam, I.G., and R.A. Dewar. 1958. "Flame Ionization Detector for Gas Chromatography." *Nature* 760.

Musculus, Mark P.B., Thierry Lachauz, Lyle M. Picket, and Cherian A. Idicheria. 2007. "End-of-Injection Over-Mixing and Unburned Hydrocarbon Emissions in Low-Temperature-Combustion Diesel Engines." *SAE International.*

Musculus, Mark, Lyle Picket, Paul Miles, John Dec, Thierry Lachaux, Caroline Genzale, Mohan Bobba, and Kyle Kattke. 2009. "In-Cylinder Processes of EGR-Diluted Low-Load, Low-Temperature Diesel Combustion." *DEER - 2009, 15th Directions in Engine Efficiency and Emissions Reduction Research.* Dearborn. 1-12.

Neely, Gary D., Shizuo Sasaki, Yiqun Huang, Jeffery A. Leet, and Daniel W. Stewart. 2005. *New Diesel Emission Control Strategy to Meet US Tier 2 Emissions Regulations.* Technical Paper, Detroit: SAE International.

NIST. 2011. *NIST Standard Reference Database Number 69.* Accessed 1 20, 2014. http://webbook.nist.gov/chemistry/.

Northrop, William F. 2010. *Particulate and Gas Phase Hydrocarbon Emissions from Partially Premixed Low Temperature Compression Ignition Combustion of Biodiesel.* Thesis, Ann Arbor: University of MIchigan.

Peeters, Jozef, and Christiaan Vinckier. 1975. "Production of chemi-ions and formation of CH and CH2 radicals in methane-oxygen and ethylene-oxygen flames." *International Symposium on Combustion* 969-977.

Pradhan, A., D.S. Shrestha, A. McAloon, W. Yee, M. Haas, and J.A. Duffield. 2011. "Energy Life-Cycle Assessment of Soybean Biodiesel Revisited." *Transactions of the ASABE* 1031-1039.

Sanchez, Fancisco Posada, Anup Bandivadekar, and John German. 2012. *Estimated Cost of Emission Reduction Technologies for Light-Duty Vehicles.* Washington DC: International Council on Clean Transportation.

Schofield, Keith. 2008. "The enigmatic mechanism of the flame ionization detector: Its overlooked implications for fossil fuel combustion modeling." *Progress in Engerg and Combustion Science* 330-350.

Schreiner, Matthias, and Howard W. Hulan. 2004. "Determination of the carbon deficiency in the flame ionization detector response of long-chain fatty acid methyl esters and dicarboxylic acid dimethyl esters." *Journal of Chromatography* 197-202.

Stivender, Donald L. 1971. "Development of a Fuel-Based Mass Emission Measurement Procedure." *Society of Automotive Engineers.*

Stone, Richard. 1999. *Introduction to Internal Combustion Engines.* Warrendale, PA: SAE International.

Twigg, Martyn V. 2009. "Cleaning the Air We Breathe – Controlling Diesel Particulate Emissions from Passenger Cars." *Platinum Metals Review* 27-34.

US EPA. 2013. *Control of Air Pollution From Motor Vehicles: Tier 3 Motor Vehicle Emission and Fuel Standards.* Federal Register, US EPA, 29816-30191.

US EPA. 1973. *Effects of FID Oven and Sample Line Temperature on the Measurement of Hydrocarbon Emissions from Diesel Engines.* Office of Air & Water Programs, Emission Control Technology Division, EPA.

US EPA. 2012. *Light-Duty Vehicle, Light-Duty Truck, and Medium-Duty Passenger Vehicle -- Tier 2 Exhaust Emission Standards.* 11 14. Accessed 1 6, 2014. http://www.epa.gov/OTAQ/standards/light-duty/tier2stds.htm.

US EPA. 2011. *Title 40: Protection of Environment: Flame-ionization detector.* Code of Federal Regulations, §1065.260.

US EPA. 2010. *Title 40: Protection of Environment: Response factor determination.* Code of Federal Regulation, §1065.845.

US EPA. 2014. *Title 40: Protection of Environment:Definitions.* Code of Federal Regulation, §86.1702-99.

Yaws, Carl L., Prasad, K. Narasimhan, and Chaitanya Gabbula. 2009. *Yaws' Handbook of Antoine Coefficients for Vapor Pressure (2nd Electronic Edition).* N/A: Knovel.

Yuan, W., A.C. Hanswen, and Q. Zhang. 2005. "Vapor pressure and normal boiling point predictions for pure methyl esters and biodiesel fuels." *FUEL* 943-950.

APPENDIX 1: Basic Performance Calculations

The global air fuel ratio was calculated by dividing the mass flow rate of air by the mass flow rate of fuel. The brake specific fuel consumption (BSFC) was calculated by dividing the flow rate of fuel by the brake power generated by the engine. The brake thermal efficiency, the fraction of energy input as fuel that is converted to useful energy by the engine, was calculated by dividing the BSFC by the lower heating value (LHV) of the fuel. The combustion efficiency, or the ratio of the energy contained in the exhaust to the energy contained in the fuel was calculated by Equation A1.1 as given by (Stivender 1971)

$$\eta_c = 100 - \left(\frac{100}{(x_{CO} + x_{CO_2} + x_{THC_1})}\right)\left(\frac{254x_{CO} + 217x_{H_2}}{h_{LHV_f} MW_f} + x_{THC_1}\right)$$

Equation A1.1

Where η_c is the combustion efficiency, x_i is the mole fraction of component *i* in the exhaust, THC_1 signifying total hydrocarbons normalized to a C_1 basis. h_{LHV_f} is the lower heating value of the fuel and MW_f is the molecular weight of the fuel. In this work x_{H_2} was not measured but calculated using a hydrogen balance as seen in Equation A1.2.

$$x_{H_2,E} = \frac{1}{2}\alpha\left(x_{CO,E} + x_{CO_2,E} - X_{CO_2,I}\right) - \left(x_{H_2O,E} - x_{H_2O,I}\right)$$

Equation A1.2

Where α is the hydrogen to carbon ratio of the fuel and $x_{i,E}$ $x_{i,I}$ are the mole fractions of component *i* in the exhaust and intake respectively. The hydrogen to carbon ratio was

measured by Paragon, the full fuel analysis report included in the Table A1 in Appendix 5. The LHV of the fuel was also given by the Paragon report, however the LHV for B100 was not given and is calculated in Appendix 3.

APPENDIX 2: Emissions Indices Calculations

The emissions index for soot, EI_{PM}, was calculated using Equation A2.1 where C_{PM} is the mass concentration of soot in the exhaust, T_{std} is standard temperature of 298 K, P_{std} is standard pressure of 1 atm, $\bar{R}$ is the universal gas constant of 8.314 J/mol-K, and AFR is the measured air fuel ratio.

$$EI_{PM} = \frac{C_{PM} T_{std} \bar{R}}{P_{std} MW_{exh}} (AFR + 1)$$

Equation A2.1

The emissions index for gaseous emission *i*, EI_i, was calculated using Equation A2.2 from Stivender, 1971 where x_i and MW_i are the mole fraction and molecular weight of component *i*, MW_f is the molecular weight of the fuel, and THC_1 is the total hydrocarbon concentration in the exhaust on a C1 basis.

$$EI_i = x_i \left(\frac{MW_i}{MW_f \left(x_{CO_2} + x_{CO} + x_{THC_1} \right)} \right)$$

Equation A2.2

THC emissions index was calculated using Equation A2.3 where 83.25 is the molecular weight for hydrocarbons on a C6 basis as defined by the EPA (Northrop 2010).

$$EI_{THC} = \frac{x_{THC_1}}{6} \left(\frac{83.25}{MW_f \left(x_{CO} + x_{CO_2} + x_{THC_1} \right)} \right)$$

Equation A2.3

NMOG emissions index was calculated by subtracting CH_4 emissions index from THC emissions index as seen in Equation A2.4. Where EI_{CH4} is calculated using Equation A2.2.

$$EI_{NMOG} = EI_{THC} - EI_{CH_4}$$

Equation A2.4

APPENDIX 3: B100 LHV Calculations

The B100 fuel was sent to Intertek for a fatty acid profile, the results of which can be found in Table A5 in Appendix 5. The fatty acid profile reported the mass fractions for a variety of compounds. Four of the acid methyl esters: Palmitic, Stearic, Elaidic, and Linolelaidic, comprised 91% of the mass. Equation A3.1 was used to determine an effective mole fraction of each component as if the fuel were made wholly of these four components.

$$x_{i_{eff}} = \frac{x_i}{\sum_{i=1}^{4} x_i}$$

Equation A3.1

Where $x_{i_{eff}}$ is the effective mole fraction for component *i*, x_i is the measured mole fraction of component *i* in the fuel. Effective molecular weight, heats of formation, carbon number, and hydrogen number for the fuel was calculated using Equation A3.2 where $Prop_{Eff}$is the effective property for the fuel (molecular weight or heat of formation) and $Prop_i$ is the property for component i. The heat of formation for each of the four components was retrieved from the National Institute of Standards and Technology (NIST) chemistry web book (NIST 2011)

$$Prop_{Eff} = \sum x_i Prop_i$$

Equation A3.2

The effective heat of vaporization for B100 was calculated using and enthalpy balance Equation A3.3 where $h^o_{f\,B100(l)}$is the effective enthalpy of formation for liquid

B100, C_{Eff} is the effective carbon number for B100, $h^o_{f\,CO_2(g)}$ is the enthalpy of formation for gaseous CO_2 H_{Eff} is the effective hydrogen number for B100, $h^o_{f\,H_2O(g)}$ is the enthalpy of formation for gaseous H_2O, and $MW_{B100_{Eff}}$ is the effective molecular weight of B100.

$$LHV_{B100} = \frac{1\left(h^o_{f\,B100(l)}\right) - \left(C_{Eff}\left(h^o_{f\,CO_2(g)}\right) + \frac{H_{Eff}}{2}\left(h^o_{f\,H_2O(g)}\right)\right)}{MW_{B100_{Eff}}}$$

Equation A3.3

APPENDIX 4: EGR Calculation

As shown in Northrop (2010), the following equations are used to calculate EGR using exhaust and intake CO2 measurements.

$$EGR_{mass} = \frac{100}{1 + \frac{MW_{air}}{MW_{exh}}\left(1 + \frac{1}{AFR_{meas}}\right)\left(\frac{100}{EGR_{mole}} - 1\right)}$$

Equation A4.1

Where MW_{air} is the molecular weight of air, 28.96 g/mol, MW_{exh} is the molecular weight of exhaust, 29.06 g/mol, $AFR_{meas}$is the global ratio found by dividing the mass flow rate of air as measured by LFE by the mass flow rate of air as measured by the coriolis meter. EGR_{mole} was found using Equation A4.2 as given by Northrop (2010).

$$EGR_{mole} = \frac{100\left(100 + X_{H2O_{Exh}}\right)X_{CO2_{int}}}{X_{H2O_{Exh}}X_{CO2_{int}} + 100X_{CO2_{Exh}}}$$

Equation A4.2

APPENDIX 5: Tables and Figures

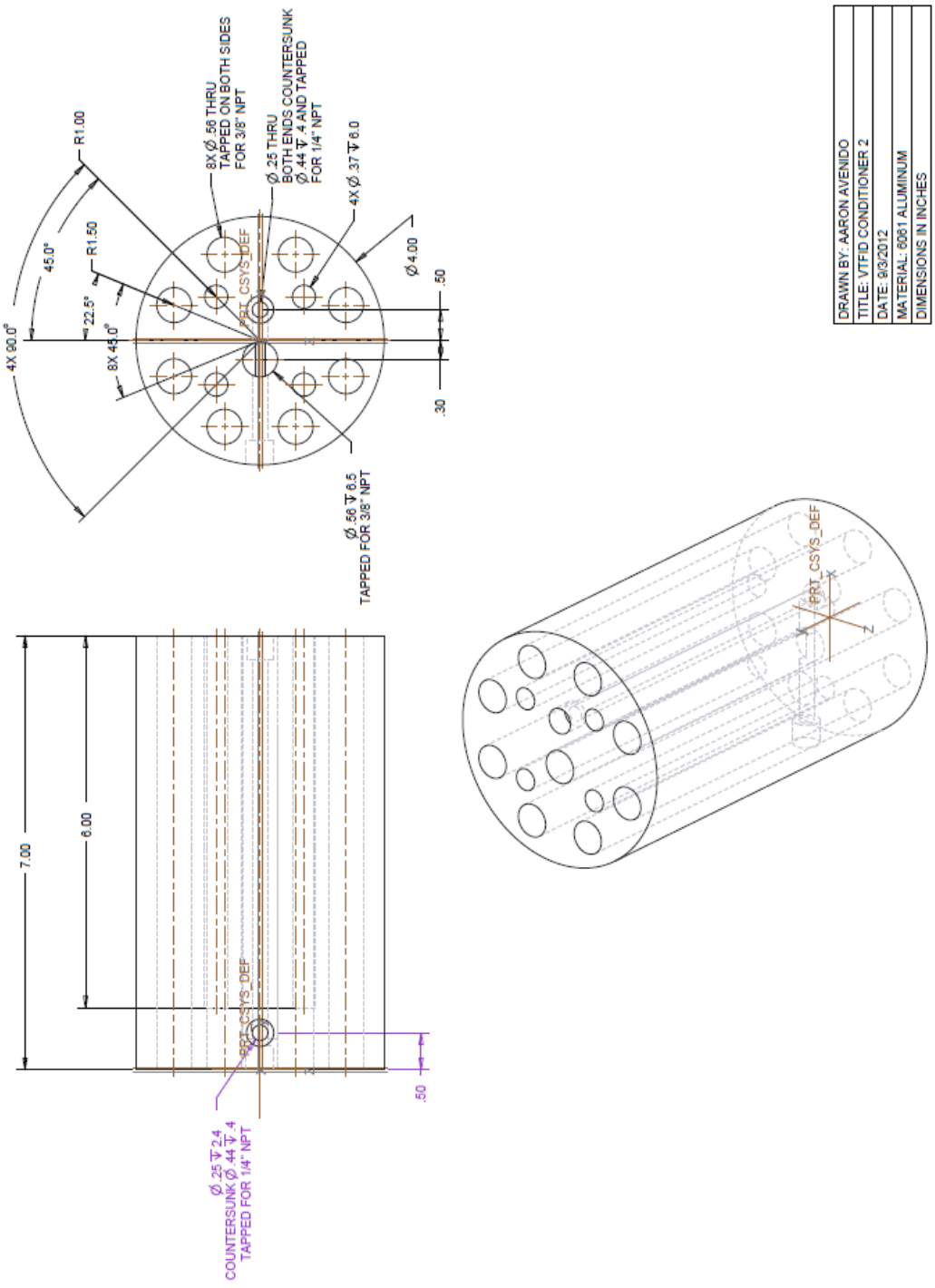

Figure A1: Sample conditioner specifications

Workorder: 186191 UNIV OF MINN-102312

Lab ID: **1861910001** Date Collected: 10/17/2012 15:00 Matrix: Diesel

Sample ID: #2 ULSD Date Received: 10/23/2012 10:09

Sample Desc: NON OXY DIESEL PO:

Parameters	Qualifier	Result Units	Dilution Factor	Reporting Limit	Result Qualifier Min	Result Qualifier Max	Analyzed	By
Distillation Degrees F								
Analytical Method: ASTM D86 [A]								
Initial Boiling Point		328.9 °F	1	0.1			10/23/2012 14:31	BAS
5.0% Recovery		368.4 °F	1	0.1			10/23/2012 14:31	BAS
10.0% Recovery		387.3 °F	1	0.1			10/23/2012 14:31	BAS
20.0% Recovery		415.8 °F	1	0.1			10/23/2012 14:31	BAS
30.0% Recovery		441.8 °F	1	0.1			10/23/2012 14:31	BAS
40.0% Recovery		465.4 °F	1	0.1			10/23/2012 14:31	BAS
50.0% Recovery		489.6 °F	1	0.1			10/23/2012 14:31	BAS
60.0% Recovery		516.1 °F	1	0.1			10/23/2012 14:31	BAS
70.0% Recovery		543.3 °F	1	0.1			10/23/2012 14:31	BAS
80.0% Recovery		574.4 °F	1	0.1			10/23/2012 14:31	BAS
90.0% Recovery		615.3 °F	1	0.1			10/23/2012 14:31	BAS
95.0% Recovery		650.4 °F	1	0.1			10/23/2012 14:31	BAS
End Point		669.7 °F	1	0.1			10/23/2012 14:31	BAS
% Overhead Recovery		97.8	1	0.1			10/23/2012 14:31	BAS
% Residue		1.5	1	0.1			10/23/2012 14:31	BAS
% Loss		0.7	1	0.1			10/23/2012 14:31	BAS
350.0°F % Recovery		1.4 mL	1	0.1			10/23/2012 14:31	BAS
400.0°F % Recovery		14.3 mL	1	0.1			10/23/2012 14:31	BAS
Individual Parameters								
Analytical Method: ASTM D4052 [A]								
API Gravity at 15.56°C		34.5 °API	1	0.1			10/23/2012 14:48	BAS
Density at 15.56°C		0.8517 g/mL	1	0.0001			10/23/2012 14:48	BAS
Spec. Grav. at 15.56°C/15.56°C		0.8525	1	0.0001			10/23/2012 14:48	BAS
Analytical Method: ASTM D445 [A]								
Viscosity, Kinematic at 40°C		2.399 mm2/sec	1	0.001			10/23/2012 14:56	AAA
Analytical Method: ASTM D240 [A]								
Gross Heating Value (BTU/lb)		19584 BTU/lb	1	175			10/24/2012 13:25	KHR
Gross Heating Value (MJ/kg)		45.552 MJ/kg	1				10/24/2012 13:25	KHR
Net Heating Value (BTU/lb)		18397 BTU/lb	1	175			10/24/2012 13:25	KHR
Net Heating Value(MJ/kg)		42.792 MJ/kg	1				10/24/2012 13:25	KHR
Analytical Method: ASTM D613 [A]								
Cetane No.		41.1	1				10/24/2012 15:30	AKL
Elemental Analysis								
Analytical Method: ASTM D5291 [A]								
Carbon (Wt%)		86.99 % m/m	1	0.05			10/24/2012 05:37	DHN
Hydrogen (Wt%)		13.01 % m/m	1	0.05			10/24/2012 05:37	DHN
Analytical Method: ASTM D5622 [A]								
Wt% of Oxygen		<0.05 % m/m	1	0.05			10/25/2012 06:16	DHN
Analytical Method: ASTM D5453 [A]								
Sulfur		4.8 ppm m/m	1	0.1			10/25/2012 12:07	AKL
Sulfur		0.00048 % m/m	1	0.00001			10/25/2012 12:07	AKL

Figure A2: ULSD Paragon Report

Table A1: ULSD Alkane profile from Intertek

Intertek

Simulated Distillation Cut Point Report

Univ of Mn ULSD 1314 1/14/2014

2014-PITT_000052-001

BP Deg F		Mass %	
97	C1-C5	0.1	%
156	C6	0.1	%
209	C7	0.2	%
258	C8	0.9	%
303	C9	1.9	%
345	C10	2.2	%
385	C11	5.6	%
421	C12	9.0	%
456	C13	11.5	%
488	C14	10.9	%
519	C15	10.3	%
548	C16	8.9	%
576	C17	8.5	%
601	C18	7.4	%
626	C19	5.8	%
651	C20	4.4	%
674	C21	3.3	%
696	C22	2.1	%
716	C23	1.2	%
736	C24	0.8	%
755	C25	0.4	%
774	C26	0.4	%
791	C27	0.2	%
808	C28	0.1	%
825	C29	0.1	%
840	C30	0.1	%

Table A2: ULSD Boiling points from Intertek

DHA Light Ends - HTSimdis Merged Boiling Point Distribution

Samplename: UMUSLD1314

DHA Datafile: C:\Users\lab.pitt@intertek.com\Documents\GC#3 Data files\umusld1314b_01142014_0910.csv
HTSD Datafile: C:\SimDist_2000\SampleData\UMUSLD1314_CDF.csv

Observed Recovery: 96.61 % @ 868.3 deg F
Used Recovery: 96.61 %

DHA Results Nonnalization Factor:
DHA Results CutOver At:

1
n-nonane 303.48 °F

Wt% Off	BP °C	BP °F	Wt% Off	BP °C	BP °F	Wt% Off	BP °C	BP °F	Wt% Off	BP °C	BP °F
0.5	34.8	94.7	26	225.1	437.2	52	269.9	517.8	78	316.6	601.8
1	100.9	213.7	27	227.1	440.7	53	271.2	520.2	79	318.6	605.5
2	118.5	245.4	28	228.9	444.0	54	272.8	523.1	80	321.1	610.0
3	144.4	292.0	29	230.4	446.7	55	274.8	526.6	81	323.6	614.5
4	160.4	320.7	30	232.1	449.7	56	276.6	529.9	82	326.4	619.5
5	170.3	338.6	31	233.9	453.0	57	278.5	533.3	83	328.9	624.0
6	176.4	349.6	32	235.4	455.7	58	280.4	536.6	84	331.1	628.0
7	181.6	358.9	33	237.0	458.6	59	282.2	540.0	85	334.1	633.5
8	185.5	365.9	34	238.9	462.0	60	284.3	543.7	86	337.4	639.4
9	189.3	372.7	35	240.7	465.3	61	286.1	547.0	87	341.1	645.9
10	192.9	379.3	36	242.4	468.2	62	287.4	549.4	88	344.1	651.5
11	195.8	384.4	37	244.3	471.7	63	289.0	552.3	89	347.9	658.3
12	198.6	389.5	38	246.0	474.8	64	290.9	555.5	90	351.9	665.4
13	200.5	392.8	39	247.8	478.0	65	292.8	559.0	91	355.9	672.7
14	202.3	396.2	40	249.5	481.1	66	294.4	562.0	92	361.2	682.2
15	204.4	400.0	41	251.2	484.1	67	296.2	565.1	93	367.3	693.1
16	206.8	404.3	42	253.0	487.3	68	298.1	568.5	94	375.2	707.4
17	209.1	408.4	43	254.3	489.7	69	300.1	572.2	95	386.3	727.3
18	211.1	412.0	44	255.8	492.5	70	301.8	575.2	96	409.3	768.7
19	213.1	415.6	45	257.5	495.5	71	303.1	577.5	97		
20	215.6	420.1	46	259.3	498.8	72	304.8	580.6	98		
21	217.5	423.5	47	261.3	502.3	73	306.8	584.2	99		
22	219.0	426.3	48	263.1	505.6	74	308.7	587.7	100		
23	220.3	428.6	49	264.8	508.6	75	310.7	591.2			
24	221.9	431.3	50	266.4	511.5	76	312.9	595.2			
25	223.3	433.9	51	268.1	514.6	77	314.9	598.9			

Figure A3: ULSD BP Distribution from Intertek

Table A3: ULSD Light ends from Intertek

Detailed Hydrocarbon Analysis Light Ends Fraction of Crude Oil
SampleName: umusdl1314b

Name	RT	Index	Mass%	CumMass%	BP °C	BP °F
n-butane	13.410	400.00	0.0100	0.0100	-0.5	31.1
i-pentane	22.470	476.70	0.0300	0.0400	27.8	82.1
n-pentane	27.210	500.00	0.0100	0.0500	36.1	96.9
2-methylpentane	41.810	574.69	0.0200	0.0700	60.3	140.5
n-hexane	48.850	600.00	0.0100	0.0800	68.7	155.7
methylcyclopentane	54.240	628.58	0.0100	0.0900	71.8	161.2
2,4-dimethylpentane	55.630	635.41	0.0100	0.1000	80.5	176.9
cyclohexane	61.450	662.07	0.0100	0.1100	80.7	177.3
2,3-dimethylpentane	64.190	673.62	0.0300	0.1400	89.8	193.6
3-methylhexane	65.950	680.78	0.0200	0.1600	91.9	197.3
2,2,4-trimethylpentane	68.550	690.96	0.0500	0.2100	99.2	210.6
n-heptane	70.960	700.00	0.0400	0.2500	98.4	209.2
methylcyclohexane	74.320	723.04	0.0600	0.3100	100.9	213.7
1c,2t,4-trimethylcyclopentane	77.940	746.62	0.0100	0.3200	116.7	242.1
2,3,4-trimethylpentane	79.580	756.92	0.0200	0.3400	113.5	236.2
toluene	80.120	760.30	0.0700	0.4100	110.6	231.1
2,3-dimethylhexane	81.330	767.69	0.0100	0.4200	115.6	240.1
2-methylheptane	82.200	772.91	0.0500	0.4700	117.7	243.8
3-ethylhexane	83.530	780.78	0.0900	0.5600	118.5	245.4
3t-ethylmethylcyclopentane	85.050	789.68	0.0200	0.5800	121.1	250.0
2t-ethylmethylcyclopentane	85.470	792.08	0.0300	0.6100	121.2	250.2
1t,2-dimethylcyclohexane	86.270	796.62	0.0300	0.6400	123.4	254.2
n-octane	86.860	800.00	0.1100	0.7500	125.7	258.2
i-propylcyclopentane	88.110	811.41	0.0100	0.7600	126.4	259.6
N3	89.400	823.10	0.0100	0.7700		
2,2-dimethylheptane	90.240	830.56	0.0300	0.8000	132.7	270.9
n-propylcyclopentane	90.780	835.40	0.1100	0.9100	131.0	267.7
4,4-dimethylheptane	91.480	841.57	0.0700	0.9800	132.9	271.2
2,6-dimethylheptane	92.210	847.87	0.0300	1.0100	135.2	275.4
ethylbenzene	92.900	853.84	0.0700	1.0800	136.2	277.2
1c,3c,5c-trimethylcyclohexane	93.280	857.12	0.0400	1.1200		
1,3-dimethylbenzene	93.890	862.30	0.2100	1.3300	139.1	282.4
4-methyloctane	94.720	869.31	0.0900	1.4200	142.4	288.4
3-methyloctane	95.500	875.89	0.0800	1.5000	144.2	291.6
1,1,2-trimethylcyclohexane	96.030	880.28	0.0400	1.5400	145.2	293.4
1,2-dimethylbenzene	96.450	883.76	0.1300	1.6700	144.4	292.0
N20	97.200	889.97	0.1600	1.8300		
N21	97.800	894.85	0.0200	1.8500		
n-nonane	98.440	900.00	0.1900	2.0400	150.8	303.5

Table A4: ULSD Cut Point Report from Intertek

DHA Light Ends - HTSimdis Merge Calculator

Cut Point Report

Samplename: UMUSLD1314

SampleInfo:

DHA Datafile: C:\Users\lab.pitt@intertek.com\Documents\GC#3 Data files\umusdl1314b_01142014_0910.csv

HTSD Datafile: C:\SimDist_2000\SampleData\UMUSLD1314_CDF.csv

Observed Recovery: 96.61 % @ 888.3 deg F

Used Recovery: 96.61 %

CutPoint Report

Start Temp degF	End Temp degF	Mass%
303	345	2.1699
345	385	5.6074
385	421	9.0390
421	455	11.5314
455	489	10.9414
489	520	10.2757
520	549	8.8895
549	576	8.4896
576	601	7.3837
601	626	5.7922
626	651	4.4280
651	674	3.2644
674	696	2.0848
696	716	1.2144
716	736	0.8464
736	755	0.3944
755	774	0.3944
774	791	0.1751
791	808	0.0569
808	825	0.0569
825	840	0.0502

Instructions:

1. Select the correct temperature units (degF or DegC)
2. Enter the Start and End Cutpoint Temps in those units
3. To implement a cutpoint that starts at a specific temperature to include the remainder of the entire sample, place the temperature in the Start Temp with an associated plus (+) sign at the end (e.g., to get the mass% recovered from 250 deg C to the end of the sample, enter 250+ in the Start Temp field). Do not place anything in the End Temp box.
4. To save this cutpoint table for future operations of this calculator, press 'Save as Default'

Table A5: Biodiesel Fatty Acid Profile

Component	Percent by Mass	Name
C14	0.06	Mytistic acid methyl ester
C16	10.14	Palmitic acid methyl ester
C16-1	0.08	Palmitoleic acid methyl ester
C17	0.10	Heptadecanoic acid methyl ester
C17-1	0.06	cis-10-heptadecenoic acid methyl ester
C18	5.10	Staeric acid methyl ester
C18-1N9T	25.20	Elaidic acid methyl ester
C18-2N6T	50.40	Linolelaidic acid methyl ester
C18-3N6T	7.23	γ-Linolenic acid methyl ester
C20	0.39	Arachidic acid methyl ester
C20-1	0.14	cis-11-eicosenoic acid methyl ester
C22	0.36	Behenic acid methyl ester
C24	0.12	Lignoceric acid methyl ester
Other Fatty Acids	0.62	

Table A6: FTIR Measurable Components

FTIR Diesel Mode	FTIR Biodiesel Mode
H2O	H2O
CO2	CO2
CO	CO
NO	NO
NO2	NO2
NH3	CH4
HNCO	C2H4
HCHO	C2H6
CH4	C3H6
C2H2	C3H8
C2H4	C4H6
C3H6	AHC
C4H6	NC8
NC8	HCHO
AHC	MECHO
SO2	C3H4O
MECHO	C3H6O
HCN	C4H6O
C2H6	C4H8O
C3H8	C7H8O
HCOOH	ME2CO
NOX	MEOH
	N2O
	NH3
	SO2
	COS
	FAME
	HCN
	HCOOH
	NOX